

1 **Universal activation mechanism of class A GPCRs**

2 Qingtong Zhou^{1,#}, Dehua Yang^{2,3,4,#}, Meng Wu^{1,3,5}, Yu Guo^{1,3,5}, Wangjing Guo^{2,3,4}, Li Zhong^{2,3,4},
3 Xiaoqing Cai^{2,4}, Antao Dai^{2,4}, Eugene Shakhnovich⁶, Zhi-Jie Liu^{1,5}, Raymond C. Stevens^{1,5}, M. Madan
4 Babu^{7*}, Ming-Wei Wang^{2,3,4,5,8*}, Suwen Zhao^{1,5*}

5 ¹Human Institute, ShanghaiTech University, 393 Middle Huaxia Road, Shanghai 201210, China

6 ²The CAS Key Laboratory of Receptor Research, Shanghai Institute of Materia Medica, Chinese
7 Academy of Sciences, 555 Zuchongzhi Road, Pudong, Shanghai 201203, China

8 ³University of Chinese Academy of Sciences, 19A Yuquan Road, Beijing 100049, China

9 ⁴The National Center for Drug Screening, Shanghai Institute of Materia Medica, Chinese Academy of
10 Sciences, 189 Guo Shou Jing Road, Shanghai 201203, China

11 ⁵School of Life Science and Technology, ShanghaiTech University, 393 Middle Huaxia Road,
12 Shanghai 201210, China

13 ⁶Department of Chemistry and Chemical Biology, Harvard University, Cambridge, MA 02138, U.S.A.

14 ⁷MRC Laboratory of Molecular Biology, Francis Crick Avenue, Cambridge CB2 0QH, U.K.

15 ⁸School of Pharmacy, Fudan University, 826 Zhangheng Road, Shanghai 201203, China

16 #These authors contributed equally to this work.

17 *Correspondences to: Suwen Zhao (zhaosw@shanghaitech.edu.cn), Ming-Wei Wang
18 (mwwang@simm.ac.cn) or Madan Babu (madanm@mrc-lmb.cam.ac.uk).

19 **Abstract**

20 Class A G protein-coupled receptors (GPCRs) influence virtually every aspect of human physiology.
21 GPCR activation is an allosteric process that links agonist binding to G protein recruitment, with the
22 hallmark outward movement of transmembrane helix 6 (TM6). However, what leads to TM6
23 movement and the key residue-level changes of this trigger remain less well understood. Here, by
24 analyzing over 230 high-resolution structures of class A GPCRs, we discovered a modular, universal
25 GPCR activation pathway that unites previous findings into a common activation mechanism, directly
26 linking the bottom of ligand-binding pocket with G protein-coupling region. We suggest that the
27 modular nature of the universal GPCR activation pathway allowed for the decoupling of the evolution
28 of the ligand binding site, G protein binding region and the residues important for receptor activation.
29 Such an architecture might have facilitated GPCRs to emerge as a highly successful family of proteins
30 for signal transduction in nature.

31 **Introduction**

32 GPCRs are membrane proteins that contain a seven-transmembrane helix (7TM) architecture¹⁻⁹. In the
33 last decade, we have witnessed a rapid development in GPCR structural biology (Figure 1a) and
34 extensive research into the mechanism by which receptors are activated by diverse ligands including
35 approved drugs¹⁻¹⁹. While these studies have provided key insights into GPCR activation mechanism
36 and implicated different parts of the receptor as being crucial for activation^{10, 20-33}, they do not fully
37 explain the pattern of conservation of residues and the number of disease-associated mutations that are
38 known to map on distinct regions of the receptor (Figure 1—figure supplement 1). Although it is well
39 established that outward movement of transmembrane helix 6 (TM6) upon ligand binding is a common
40 feature of receptor activation^{3-5, 20-23}, what leads to the movement of TM6, are they conserved, how the
41 other helices are rearranged to facilitate this movement, and the key residue level changes of this
42 trigger all remain less well understood (Figure 1b). Receptor activation requires global reorganization
43 of residue contacts as well as water-mediated interactions¹⁸⁻¹⁹. Since prior studies primarily
44 investigated conformational changes through visual inspection²⁰⁻²² or through the presence or absence
45 of non-covalent contacts between residues⁸⁻¹⁰, we reasoned that one could gain comprehensive
46 knowledge about mechanism of receptor activation by developing approaches that can capture not just
47 the presence or absence of a contact but also subtle, and potentially important alterations in
48 conformations upon receptor activation.

49 **Results**

50 **A residue-residue contact score-based framework to characterize GPCR conformational changes**

51 To address this, we developed an approach to rigorously quantify residue contacts in proteins
52 structures and infer statistically significant conformational changes. We first defined a residue-residue
53 contact score (RRCS) which is an atomic distance-based calculation that quantifies the strength of
54 contact between residue pairs³⁴ by summing up all possible inter-residue heavy atom pairs (Figure 2a

55 and Figure 2—figure supplement 1a). We then defined Δ RRCS, which is the difference in RRCS of a
56 residue pair between any two conformational states of a receptor that quantitatively describes the
57 rearrangements of residue contacts (Figure 2b and Figure 2—figure supplement 1b). While RRCS can
58 be 0 (no contact) or higher (stronger contact), Δ RRCS can be negative (loss in strength of residue
59 contact), positive (gain in strength of residue contact) or 0 (no change in strength of residue contact).
60 To capture the entirety of conformational changes in receptor structure upon activation, we computed
61 the Δ RRCS between the active and inactive state of a receptor and defined two types of conformational
62 changes (Figure 2c): (i) switching contacts: these are contacts that are present in the inactive state but
63 lost in the active state (or *vice versa*) such as loss of intrahelical contacts between D/E^{3×49} (GPCRdb
64 numbering³⁵) and R^{3×50}, and gain of interhelical hydrophobic contacts between residues at 3×40 and
65 6×48 upon receptor activation; and (ii) repacking contacts: these are contacts that result in an increase
66 or decrease in residue packing such as the decreased packing of intrahelical sidechain contacts between
67 W^{6×48} and F^{6×44}, and the increase in interhelical residue packing due to the translocation of N^{7×49}
68 towards D^{2×50} upon receptor activation. In this manner, we quantified the global, local, major and
69 subtle conformational changes in a systematic way (*i.e.*, interhelical and intrahelical, switching and
70 repacking contacts).

71 We then analysed 234 structures of 45 class A GPCRs that were grouped into three categories (Figure
72 1a): (i) antagonist- or inverse agonist-bound (inactive; 142 structures from 38 receptors); (ii) both
73 agonist- and G protein/G protein mimetic-bound (fully active; 27 structures from 8 receptors); and (iii)
74 agonist-bound (intermediate; 65 structures from 15 receptors). Among them, six receptors [rhodopsin
75 (bRho), β_2 -adrenergic receptor (β_2 AR), M2 muscarinic receptor (M2R), μ -opioid receptor (μ OR),
76 adenosine A_{2A} receptor (A_{2A}R) and κ -opioid receptor (κ -OR)] have both inactive- and active-state
77 crystal structures available. Given that Δ RRCS can capture major and subtle conformational changes,
78 we computed RRCS for all structures and Δ RRCS for the six pairs of receptors and investigated the

79 existence of a common activation pathway (*i.e.*, a common set of residue contact changes) across class
80 A GPCRs. Two criteria (Figure 2d; further details in Methods) were applied to identify conserved
81 rearrangements of residue contacts: (i) equivalent residue pairs show a similar and substantial change
82 in RRCS between the active and inactive state structures of each of the six receptors (*i.e.*, the same
83 sign of Δ RRCS and $|\Delta$ RRCS| > cut-off for all receptors) and (ii) family-wide comparison of the RRCS
84 for the 142 inactive and 27 active state structures shows a statistically significant difference ($P < 0.001$;
85 two sample *t*-test). This allowed us to reliably capture both the major rearrangements as well as subtle
86 but conserved conformational changes at the level of individual residues in diverse GPCRs in a
87 statistically robust and significant manner. Consistent with this, a comparison with earlier studies
88 revealed that the RRCS based approach is able to capture a larger number of conserved large-scale and
89 subtle changes in residues contacts (Figure 2d) that would have been missed by visual inspection or
90 residue contact presence/absence criteria alone (see Methods for conceptual advance of this approach
91 and detailed comparison)^{8, 10, 20-22}.

92 **Discovery of the universal and conserved receptor activation pathway**

93 Remarkably, for the first time, our analysis of the structures allowed the discovery of a universal and
94 conserved activation pathway that directly links ligand-binding pocket and G protein-coupling regions
95 in class A GPCRs (Figure 3). The pathway is comprised of 34 residue pairs (formed by 35 residues)
96 with conserved rearrangement of residue contacts upon activation (Figure 2d), connecting several well-
97 known but structurally and spatially disconnected motifs (CWxP^{11, 20, 33}, PIF^{3, 36}, Na⁺ pocket^{19, 24, 33},
98 NPxxY^{20, 23} and DRY^{11, 14, 37}) all the way from the extracellular side (where the ligand binds) to the
99 intracellular side (where the G protein binds). Inspection of the rewired contacts as a Δ RRCS network
100 reveals that the conserved receptor activation pathway is modular and involves conformational
101 changes in four layers. In layer 1, there is a conserved signal initiation step involving changes in
102 residue contacts at the bottom of the ligand-binding pocket and Na⁺ pocket. In layer 2, critical

103 hydrophobic contacts are broken (*i.e.*, opening of the hydrophobic lock). In layer 3, microswitch
104 residues (6×37, Y^{7×53}) are rewired and in layer 4, the residue R^{3×50} and G protein contacting positions
105 are rewired, making them competent to bind to G protein on the cytosolic side (Figure 3). Strikingly,
106 recently released cryo-EM structures of three receptors (5-HT_{1B}, A₁R and μOR) in complex with G_{i/o}³⁸
107 also support the conservation of contacts involving these 34 residue pairs (Figure 4, Figure 4—figure
108 supplements 1 and 2). These observations highlight the conserved and universal nature of a previously
109 undescribed activation pathway linking ligand binding to G protein coupling, regardless of the
110 subtypes of intracellular effectors (*i.e.*, G_s, G_{i/o}, arrestin or G protein mimetic nanobody/peptide, Figure
111 4a). Collectively, these findings illustrate how a combination of intrahelical and interhelical switching
112 contacts as well as repacking contacts underlies the universal activation mechanism of GPCRs.

113 **Molecular insights into the key steps of the universal receptor activation pathway**

114 Receptor activation is triggered by ligand binding and is characterised by movements of different
115 transmembrane helices. How does ligand-induced receptor activation connect the different and highly
116 conserved motifs, rewire residue contacts and result in the observed changes in transmembrane helices?
117 To this end, we analysed the universal activation pathway in detail and mapped, where possible, how
118 they influence helix packing, rotation and movement (Figure 3). A qualitative analysis suggests the
119 presence of four layers of residues in the activation pathway linking the ligand binding residues to the
120 G protein binding region.

121 Layer 1: We did not see a single ligand-residue contact that exhibits conserved rearrangement, which
122 accurately reflects the diverse repertoire of ligands that bind GPCRs^{2, 12, 34} (Figure 3—figure
123 supplement 1). Instead, as a first common step, binding of diverse extracellular agonist converges to
124 trigger an identical alteration of the transmission switch (3×40, 5×51, 6×44 and 6×48)^{1, 21} and Na⁺
125 pocket (2×50, 3×39, 7×45 and 7×49)^{19, 24, 33}. Specifically, the repacking of an intrahelical contact
126 between residues at 6×48 and 6×44, together with the switching contacts of residue at 3×40 towards

127 6×48 and residue at 5×51 towards 6×44, contract the TM3-5-6 interface in this layer. This
128 reorganization initializes the rotation of the cytoplasmic end of TM6. The collapse of Na⁺ pocket^{19,24,}
129 ³²⁻³³ leads to a denser repacking of the four residues (2×50, 3×39, 7×45 and 7×49), initiating the
130 movement of TM7 towards TM3.

131 Layer 2: In parallel with these movements, two residues (6×40 and 6×41) switch their contacts with
132 residue at 3×43, and form new contacts instead with residues at 5×58 and 5×55, respectively.
133 Residues at 3×43, 6×40 and 6×41 are mainly composed of hydrophobic amino acids and referred as
134 hydrophobic lock^{22, 28, 39}. Its opening loosens the packing of TM3-TM6 and facilitates the outward
135 movement of the cytoplasmic end of TM6, which is necessary for receptor activation. Additionally,
136 N^{7×49} develops contacts with residue at 3×43 from nothing, facilitating the movement of TM7 towards
137 TM3.

138 Layer 3: Upon receptor activation, Y^{7×53} loses its interhelical contacts⁸ with residues at 1×53 and
139 8×50, and forms new contacts with residues at 3×43, 3×46 and R^{3×50}, which were closely packed
140 with residues in TM6. Thus, the switching of contacts by Y^{7×53} strengthens the packing of TM3-TM7,
141 while the packing of TM3-TM6 is further loosened with the outward movement of TM6.

142 Layer 4: Finally, the restrains on R^{3×50}, including more conserved, local intrahelical contacts with
143 D(E)^{3×49} and less conserved ionic lock with D(E)^{6×30}, are eliminated^{11, 14, 37} and R^{3×50} is released.
144 Notably, the switching contacts between R^{3×50} and residue at 6×37 are essential for the release of
145 R^{3×50}, which breaks the remaining contacts between TM3 and TM6 in the cytoplasmic end and drives
146 the outward movement of TM6. The rewired contacts of R^{3×50} and other G protein contacting positions
147 (3×53, 3×54, 5×61 and 6×33) make the receptor competent to bind to G protein on the cytosolic side.

148 Together, these findings demonstrate that the intrahelical/interhelical and switching/repacking contacts
149 between residues is not only critical to reveal the continuous and modular nature of the activation
150 pathway, but also to link residue-level changes to transmembrane helix-level changes in the receptor.

151 **Universal activation pathway induced changes in transmembrane helix packing in GPCRs**

152 To capture the patterns in the global movements of transmembrane helices, 8 residue pairs were
153 chosen to describe the interhelical contacts between the cytoplasmic end of TM3 and TM6 as well as
154 TM3 and TM7 (Figure 5a). Analysis of the $RRCS_{TM3-TM7}$ (X-axis) and $RRCS_{TM3-TM6}$ (Y-axis) for each
155 of the 234 class A GPCR structures revealed distinct compact clusters of inactive and active states.
156 Surprisingly, the inactive state has zero or close to zero $RRCS_{TM3-TM7}$ regardless of the wide
157 distribution of $RRCS_{TM3-TM6}$. In contrast, the active state has a high $RRCS_{TM3-TM7}$ and strictly zero
158 $RRCS_{TM3-TM6}$. Thus, receptor activation from inactive to active state occurs as a harmonious process of
159 interhelical contacts changes: elimination of TM3-TM6 contacts, formation of TM3-TM7 contacts and
160 repacking of TM5-TM6 (Figure 5b and Figure 5—figure supplement 1). In terms of global
161 conformational changes, the binding of diverse agonists converges to trigger outward movement of the
162 cytoplasmic end of TM6 and inward movement of TM7 towards TM3^{8, 20, 23}, thereby creating an
163 intracellular crevice for G protein coupling (Figure 5b).

164 **Experimental validation for the modular nature of the universal activation pathway**

165 Based on the knowledge of the universal activation pathway, one would expect that mutations of
166 residues in the pathway are likely to severely affect receptor activation. The two extreme consequences
167 are constitutive activation (without agonist binding) or inactivation (abolished signalling). To
168 experimentally test this hypothesis, we systematically designed site-directed mutagenesis for residues
169 in the pathway on a prototypical receptor A_2AR , aiming to create constitutively activating/inactivating
170 mutations (CAM/CIM), by promoting/blocking residue and helix level conformational changes
171 revealed in the pathway. 6/15 designed CAMs and 15/20 designed CIMs were validated by functional

172 cAMP accumulation assays, and none of them were reported before for A_{2A}R (Figure 6, Figure 6—
173 figure supplement 1 and Figure 6—source data 1). The design of functional active/inactive mutants has
174 been very challenging. However, the knowledge of universal activation pathway of GPCRs presented
175 here greatly improves the success rate. The mechanistic interpretation of 21 successful predicted
176 mutants is explained as below. We discuss the 14 unsuccessful predictions in the Figure 6—source
177 data 2.

178 In layer 1, the mutation I92^{3×40}N likely stabilizes the active state by forming amide- π interactions with
179 W246^{6×48} and hydrogen bond with the backbone of C185^{5×461}, which rewires the packing at the
180 transmission switch and initiates the outward movement of the cytoplasmic end of TM6; this mutation
181 elevated the basal cAMP level by 7-fold. Conversely, I92^{3×40}A would reduce the favourable contacts
182 with W^{6×48} upon activation, which retards the initiation of the outward movement of TM6; this
183 mutation resulted in a decrease in both basal cAMP level [71% of wild-type (WT)] and agonist
184 potency (8-fold). Another example is the residue at 6×44, the mutation F242^{6×44}R would stabilize the
185 inactive state by forming salt bridge with D52^{2×50}, which blocks the rotation of TM6 and thus
186 abolishes G_s coupling; indeed this mutation greatly reduced basal cAMP level (to 63% WT) and
187 agonist potency (by 374-fold). In contrast, F242^{6×44}A would reduce contacts with W246^{6×48}, loosen
188 TM3-TM6 contacts, diminish the energy barrier of TM6 release and make outward movement of TM6
189 easier; consistently this mutation elevated the basal cAMP level (by 2-fold) and increased the agonist
190 potency (by 8-fold). Mutations of residues forming the Na⁺ pocket, such as D52^{2×50}A and N280^{7×45}R,
191 would destroy the hydrogen bond network at the Na⁺ pocket and retard the initiation of the inward
192 movement of TM7. These mutations completely abolished agonist potency and greatly reduced the
193 basal cAMP level (to 80% and 78% of WT, respectively).

194 In layer 2, the mutations L95^{3×43}A/R and I238^{6×40}Y would loosen the hydrophobic lock, weaken TM3-
195 TM6 contacts, promote the outward movement of cytoplasmic end of TM6 and eventually make
196 receptor constitutively active; this is reflected by remarkably high basal cAMP production (28-, 2- and
197 11-fold increase, respectively). Notably, mutations at/near the Na⁺ pocket, L48^{2×46}R and N284^{7×49}K,
198 could lock the Na⁺ pocket at inactive packing mode by introducing salt bridge with D52^{2×50}, thus
199 block the inward movement of TM7 towards TM3. As expected, these mutations completely abolished
200 agonist potency. The CIMs at/near the Na⁺ pocket (from both layer 1 and 2) reflect the subtle inward
201 movement of TM7 towards TM3 is essential for receptor activation, which is often underappreciated
202 and overshadowed by the movement of TM6. In line with this, two mutations on TM7, N284^{7×49}A and
203 Y288^{7×53}A, attenuate the TM3-TM7 contacts upon activation and completely abolished or greatly
204 reduced (by 16-fold) agonist potency, respectively.

205 In layer 3, I98^{3×46}A likely reduces contacts with Y288^{7×53}, weakens the packing between TM3-TM7,
206 and retards the movement of TM7 towards TM3; similarly, L235^{6×37}A would reduce contacts with
207 F201^{5×62}, weaken the packing between TM5-TM6, and makes the TM6 movement towards TM5 more
208 difficult. In line with the interpretation, these mutations resulted in reduced basal cAMP level (72%
209 and 71% WT, respectively) and decreased agonist potency (23- and 4-fold, respectively). These results
210 are consistent with previous findings on vasopressin type-2 receptor (V2R)⁸. In layer 4, D101^{3×49}N
211 likely diminishes its intrahelical interactions with R102^{3×50} and thus makes the release of the latter
212 easier, which in turn promotes the G protein recruitment. Consistent with this possibility, this mutation
213 led to a greatly elevated basal cAMP level (8-fold).

214 Despite these A_{2A}R mutants greatly affect receptor activation, our radioligand binding assay shows
215 that they generally retain the agonist binding ability, with the exception of two CIMs: W246^{6×48}A and
216 N284^{7×45}K (Figure 6b, c and Figure 6—source data 1). This suggests that the universal activation

217 pathway is modular and that such an organization allows for a significant number of residues involved
218 in agonist binding to be uncoupled from receptor activation/inactivation and G protein binding.

219 **The universal activation pathway allows mechanistic interpretation of mutations**

220 Four hundred thirty five disease-associated mutations were collected, among which 28% can be
221 mapped to the universal activation pathway, much higher than that to the ligand-binding and G
222 protein-binding regions (20% and 7%, respectively) (Figure 7a, b). Furthermore, 272 CAMs/CIMs
223 from 41 receptors (Figure 7c) were mined from the literature for the 14 hub residues (*i.e.*, residues that
224 have more than one edges in the pathway).

225 The average number of disease-associated mutations in the universal activation pathway is much
226 higher than that of ligand-binding pocket, G protein-binding pocket, and residues in other regions (2.5-,
227 3.5- and 3.5-fold, respectively), reflecting the enrichment of disease-associated mutations on the
228 pathway (Figure 7a). Within the universal activation pathway, the enrichment of disease mutations and
229 CAMs/CIMs in layers 1 and 2 is noteworthy, which highlights the importance of signal initiation and
230 hydrophobic lock opening, and further supports the modular and hierarchical nature of GPCR
231 activation (Figures 3 and 5b). Notably, for certain residues, such as D^{2×50} and Y^{7×53}, only loss-of-
232 function disease mutations or CIMs were observed (Figures 7 and 8b), implying they are indispensable
233 for receptor activation and the essential role of TM7 movement (Figures 3 and 5).

234 The functional consequence of these single point mutations can be rationalized by analysing if they are
235 stabilizing/destabilizing the contacts in the universal activation pathway or promoting/retarding the
236 required helix movement upon activation (Figure 7b and Figure 7—figure supplement 1). For example,
237 I130^{3×43}N/F (in layer 2 of the universal activation pathway) in V2R was reported as a gain-/loss-of-
238 function mutation that causes nephrogenic syndrome of inappropriate antidiuresis⁴⁰ or nephrogenic
239 diabetes insipidus⁴¹, respectively. I130^{3×43}N/F likely loosens/stabilizes the hydrophobic lock,
240 weakens/strengthens the TM3-TM6 packing and leads to constitutively active/inactive receptors.

241 Another example is T58^{1×53}M in rhodopsin, which was reported as a loss-of-function mutation that
242 causes retinitis pigmentosa 4⁴². T58^{1×53}M likely increases hydrophobic contacts with Y306^{7×53} and
243 P303^{7×50}, which retards the inward movement of TM7 towards TM3 and eventually decreases G
244 protein recruitment. As in the case of disease-associated mutations, CAMs/CIMs that have been
245 previously reported in the literature can also be interpreted by the framework of universal activation
246 pathway (Figure 7—figure supplement 1b). For example, F248^{6×44}Y in CXCR4²⁸ was reported as a
247 CIM. This residue likely forms hydrogen bond with S123^{3×39}, which blocks the rotation of the
248 cytoplasmic end of TM6, and decreases G protein engagement.

249 Not surprisingly, the 35 residues constituting the pathway are highly conserved across class A GPCRs,
250 dominated by physiochemically similar amino acids (Figure 7—figure supplement 2). The average
251 sequence similarity of these positions across 286 non-olfactory class A receptors is 66.2%,
252 significantly higher than that of ligand-binding pockets (31.9%) or signalling protein-coupling regions
253 (35.1%). Together, these observations suggest that the modular and hierarchical nature of the
254 activation pathway allows decoupling of the ligand-binding pocket, G protein-binding pocket and the
255 residues contributing to the universal activation mechanism. Such an organization of the receptor
256 might facilitate the uneven sequence conservation between different regions of GPCRs, confers their
257 functional diversity in ligand recognition and G protein binding while still retaining a common
258 activation mechanism.

259 **Discussion**

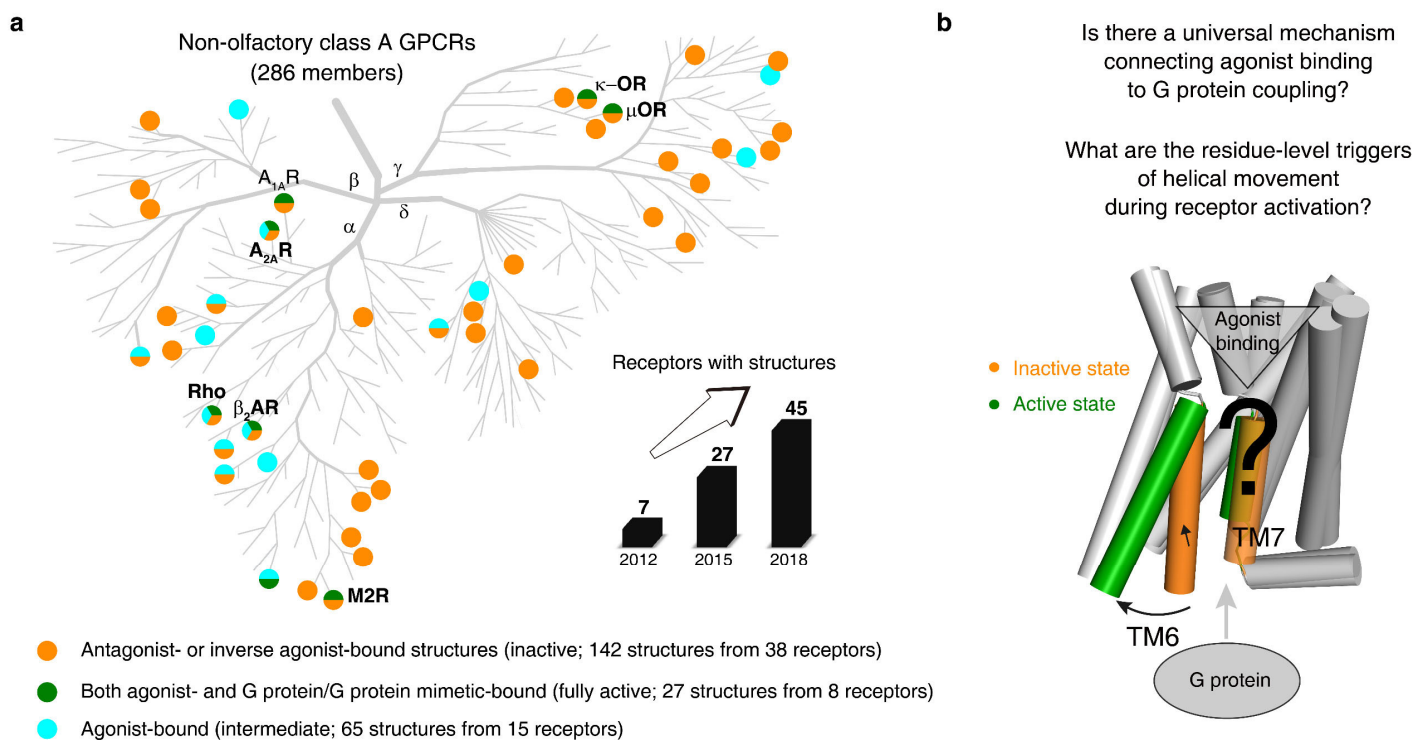
260 Using a novel, quantitative residue contact descriptor, RRCS, and a family-wide comparison across
261 234 structures from 45 class A GPCRs, we reveal a universal, modular activation pathway that directly
262 links ligand-binding pocket and G protein-coupling regions. Key residues that connect the different
263 modules allows for the decoupling of a large number of residues in the ligand-binding site, G protein

264 contacting region and residues involved in the activation pathway. Such an organization may have
265 facilitated the rapid expansion of GPCRs through duplication and divergence, allowing them to evolve
266 independently and bind to diverse ligands due to removal of the constraint (i.e. between a large number
267 of ligand binding residues and those involved in receptor activation). This model unifies many
268 previous important motifs and observations on GPCR activation in the literature (CWxP^{11, 20, 33}, DRY^{11,}
269 ^{14, 37}, Na⁺ pocket^{19, 24, 33}, NPxxY^{20, 23}, PIF^{3, 36} and hydrophobic lock^{22, 28, 39}] and is consistent with
270 numerous experimental findings^{21-22, 28, 33, 39}.

271 We focused on the universal activation pathway (*i.e.*, the common part of activation mechanism shared
272 by all class A GPCRs and various intracellular effectors) in this study. Obviously, individual class A
273 receptor naturally has its intrinsic activation mechanism(s), as a result of the diversified sequences,
274 ligands and physiological functions. Indeed, receptor-specific activation pathways (including
275 mechanisms of orthosteric, positive or negative allosteric modulators, biased signalling/selectivity of
276 downstream effectors)^{5, 9, 17, 43-48} have been revealed by both experimental studies including
277 biophysical (such as X-ray, cryo-EM, NMR, FRET/BRET, DEER)^{2, 9, 14, 27, 33, 43, 49-52}, biochemical^{28, 39}
278 and computational approaches (such as evolutionary trace analysis^{26, 30} and molecular dynamics
279 simulations^{16, 25, 31, 53}), especially for the prototypical receptors such as rhodopsin, β_2 -adrenergic and
280 A_{2A} receptors. These studies demonstrated the complexity and plasticity of signal transduction of
281 GPCRs. The computational framework we have developed may assist us in better understanding the
282 mechanism of allosteric modulators, G protein selectivity and diverse activation processes via
283 intermediate states as more GPCR structures become available. While we interpret the changes as a
284 linear set of events, future studies aimed at understanding dynamics could provide further insights into
285 how the common activation mechanism operates in individual receptors.

286 Given the universal and conserved nature of the pathway, we envision that the knowledge of the
287 common activation pathway can not only be used to mechanistically interpret the effect of mutations in
288 biological and pathophysiological context⁵⁴ but also to rationally introduce mutations in other

289 receptors by promoting/blocking residue and helix level movements that are essential for activation.
290 Such protein engineering approaches can obtain receptors in specific conformational states to
291 accelerate structure determination studies using X-ray crystallography or electron microscopy in future.
292 The approach developed here can be readily adapted to map allosteric pathways and reveal
293 mechanisms of action for other key biological systems such as kinases, ion channels and transcription
294 factors.



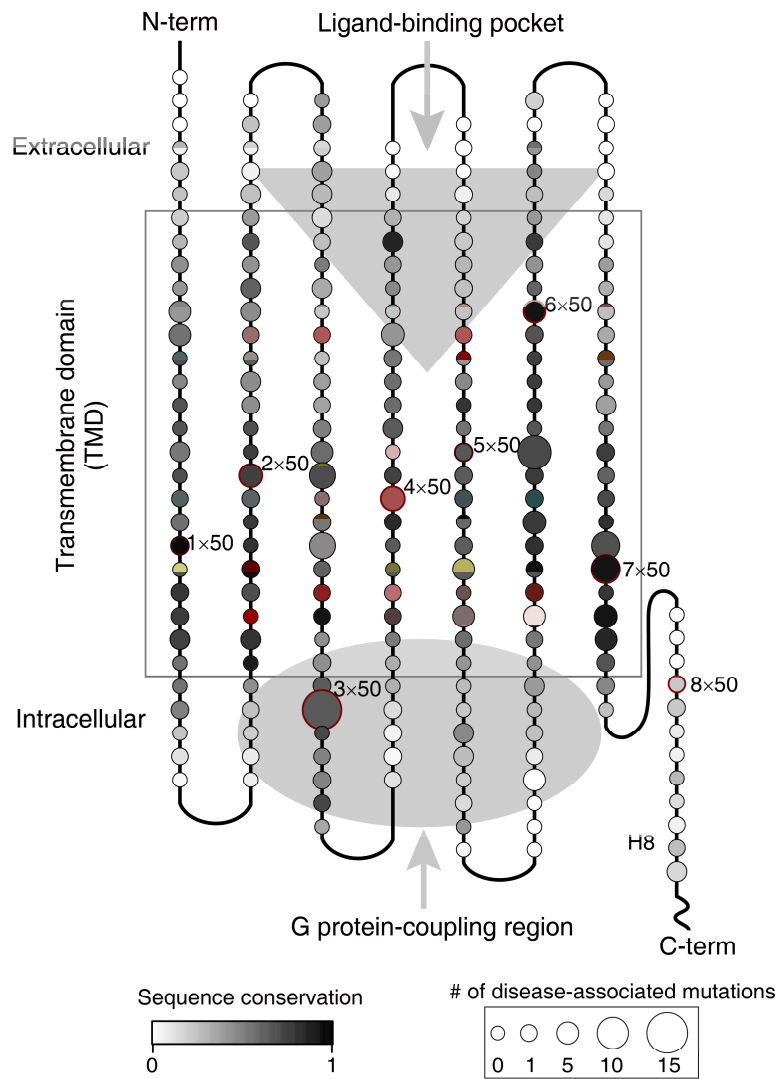
295 **Figure 1. An increasing number of reported class A GPCR structures facilitates studies on**
296 **universal activation mechanism. a, Distribution of structures in different states in the non-olfactory**
297 **class A GPCR tree as of October 1, 2018. b, Universal GPCR activation mechanism and the residue-**
298 **level triggers are not well understood.**

299 The following source data and figure supplement are available for figure 1:

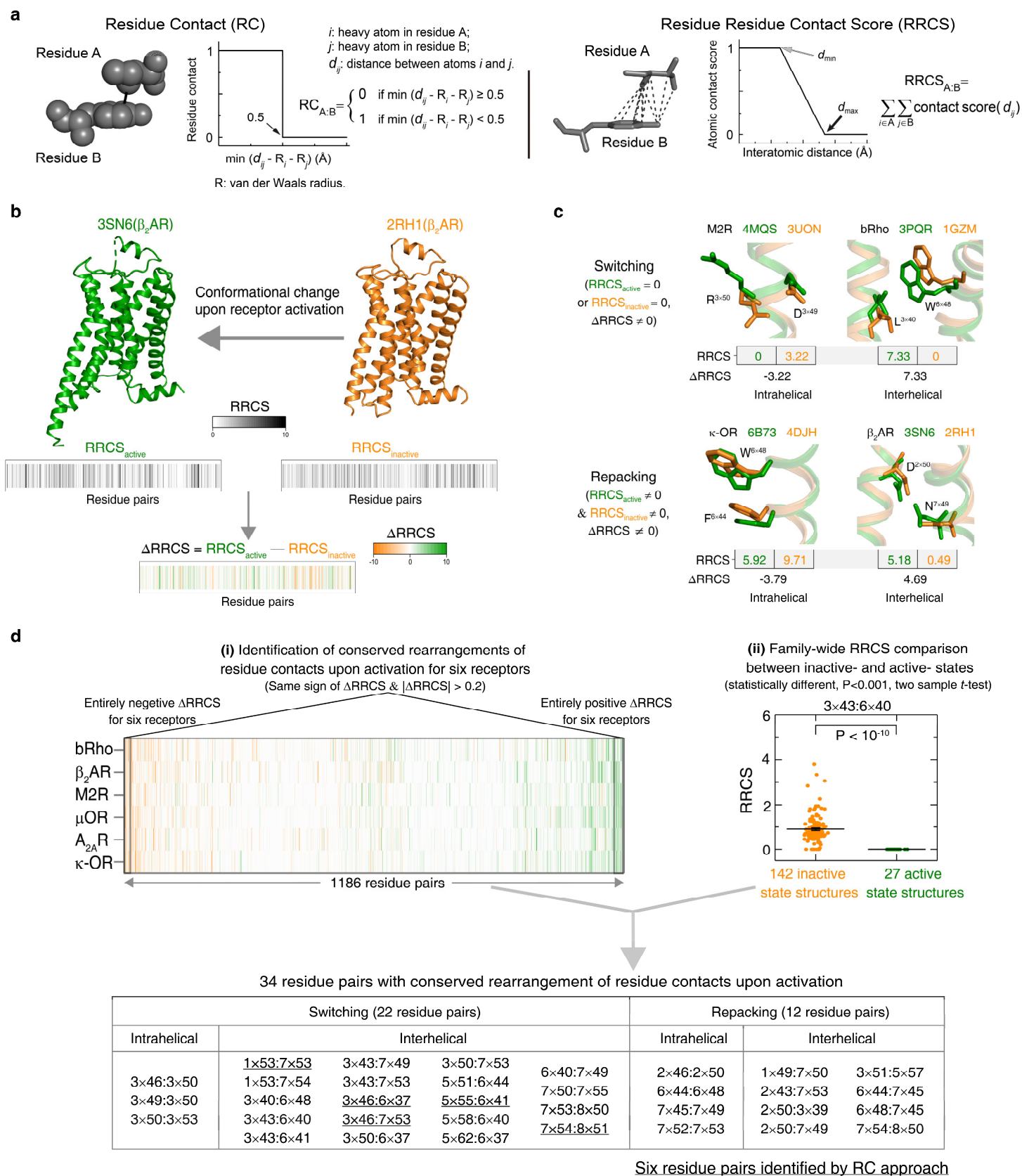
300 **Source data 1.** The released class A GPCR structures (as of October 1, 2018).

301 **Source data 2.** Disease mutations occurred in class A GPCRs.

302 **Figure supplement 1.** The pattern of conservation of residues and the map of number of disease-
303 associated mutations on human class A GPCRs.



304
305 **Figure 1—figure supplement 1. The pattern of conservation of residues and the map of number**
306 **of disease-associated mutations on human class A GPCRs.** The alignment of 286 non-olfactory,
307 class A human GPCRs were obtained from the GPCRdb^{35, 54-55} and sent for the sequence conservation
308 score calculation for all residue positions by the Protein Residue Conservation Prediction⁵⁶ tool with
309 scoring method “property entropy”⁵⁷. To obtain disease-associated mutations, we performed database
310 integration and literature investigation for all 286 non-olfactory class A GPCRs. Four commonly used
311 databases (UniProt⁵⁸, OMIM⁵⁹, Ensembl⁶⁰ and GPCRdb⁵⁴⁻⁵⁵) were first filtered by disease mutations
312 and then merged. Finally, we collected 435 disease mutations from 61 class A GPCRs (Figure 1—
313 Source data 2).



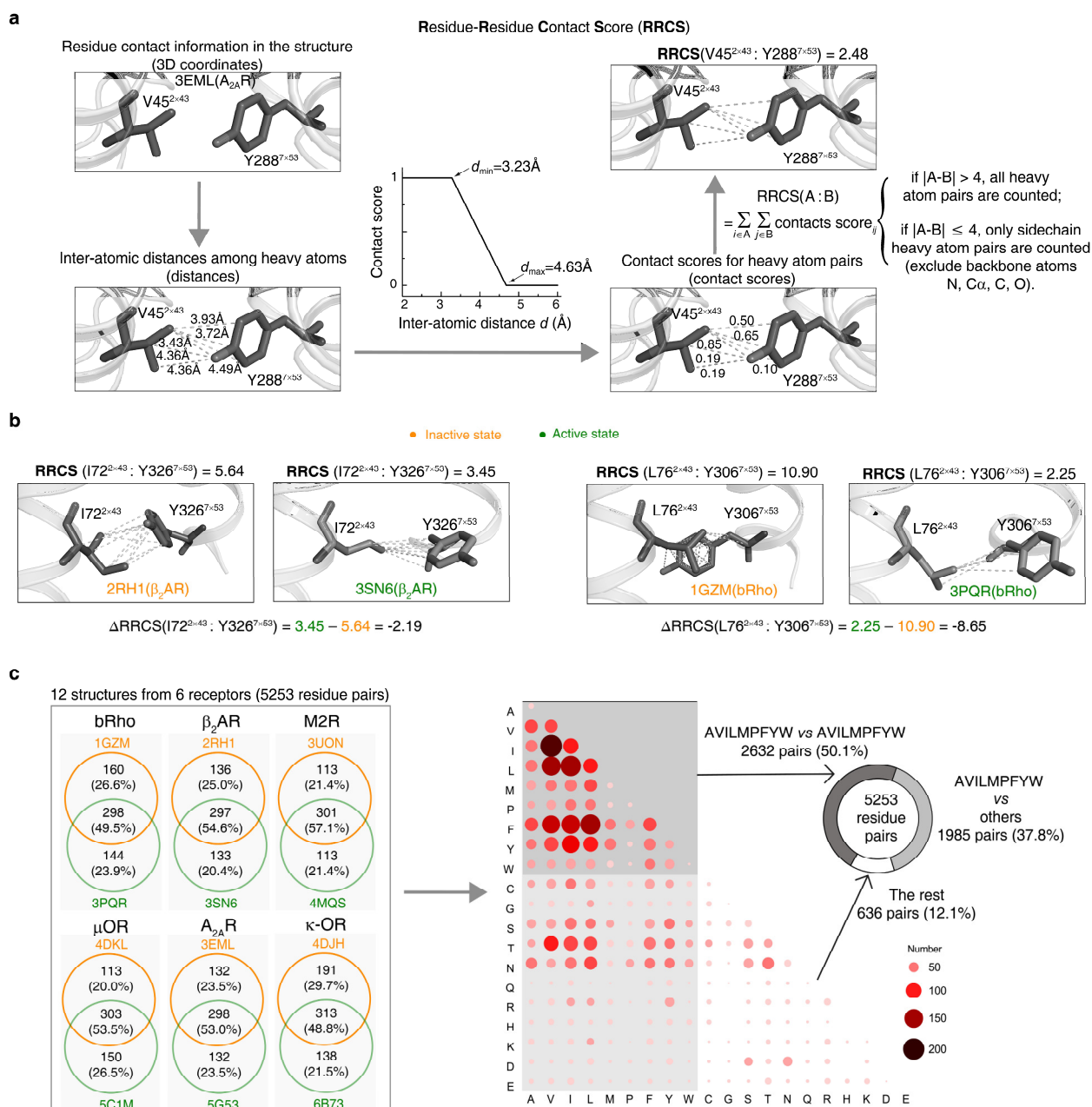
315 **Figure 2. Understanding GPCR activation mechanism by RRCS and Δ RRCS.** **a**, Comparison of
316 residue contact (RC)⁸ and residue residue contact score (RRCS) calculations. RRCS can describe the
317 strength of residue-residue contact quantitatively in a much more accurate manner than the Boolean
318 descriptor RC. **b**, RRCS and Δ RRCS calculation for a pair of active and inactive structures can capture
319 receptor conformational change upon activation. **c**, Two types of conformational changes (*i.e.*,
320 switching and repacking contacts) can be defined by RRCS to quantify the global, local, major and
321 subtle conformational changes in a systematic way. **d**, Two criteria of identifying conserved residue
322 rearrangements upon receptor activation by RRCS and Δ RRCS. 34 residues pairs were identified
323 based on the criteria (please see Methods, Figure 2—Source data 1 and 2 for details), only 6 of them
324 were discovered before⁸.

325 The following source data and figure supplement are available for figure 2:

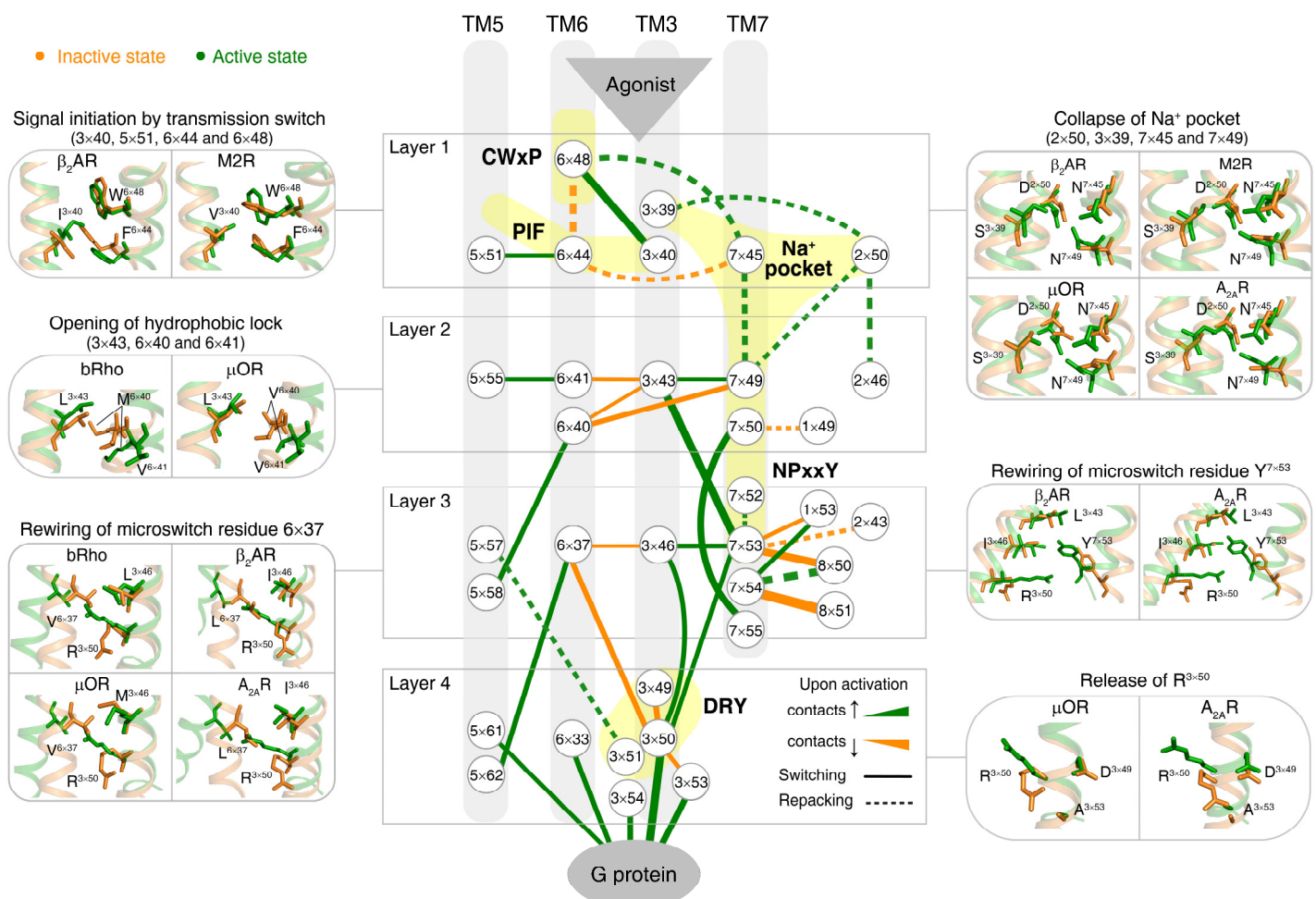
326 **Source data 1.** Calculated RRCS of 34 residue pairs constituting the universal activation pathway for
327 released class A GPCR structures.

328 **Source data 2.** Thirty-four residue pairs shown conserved rearrangements of residue contacts upon
329 activation.

330 **Figure supplement 1.** Calculation of RRCS and Δ RRCS.



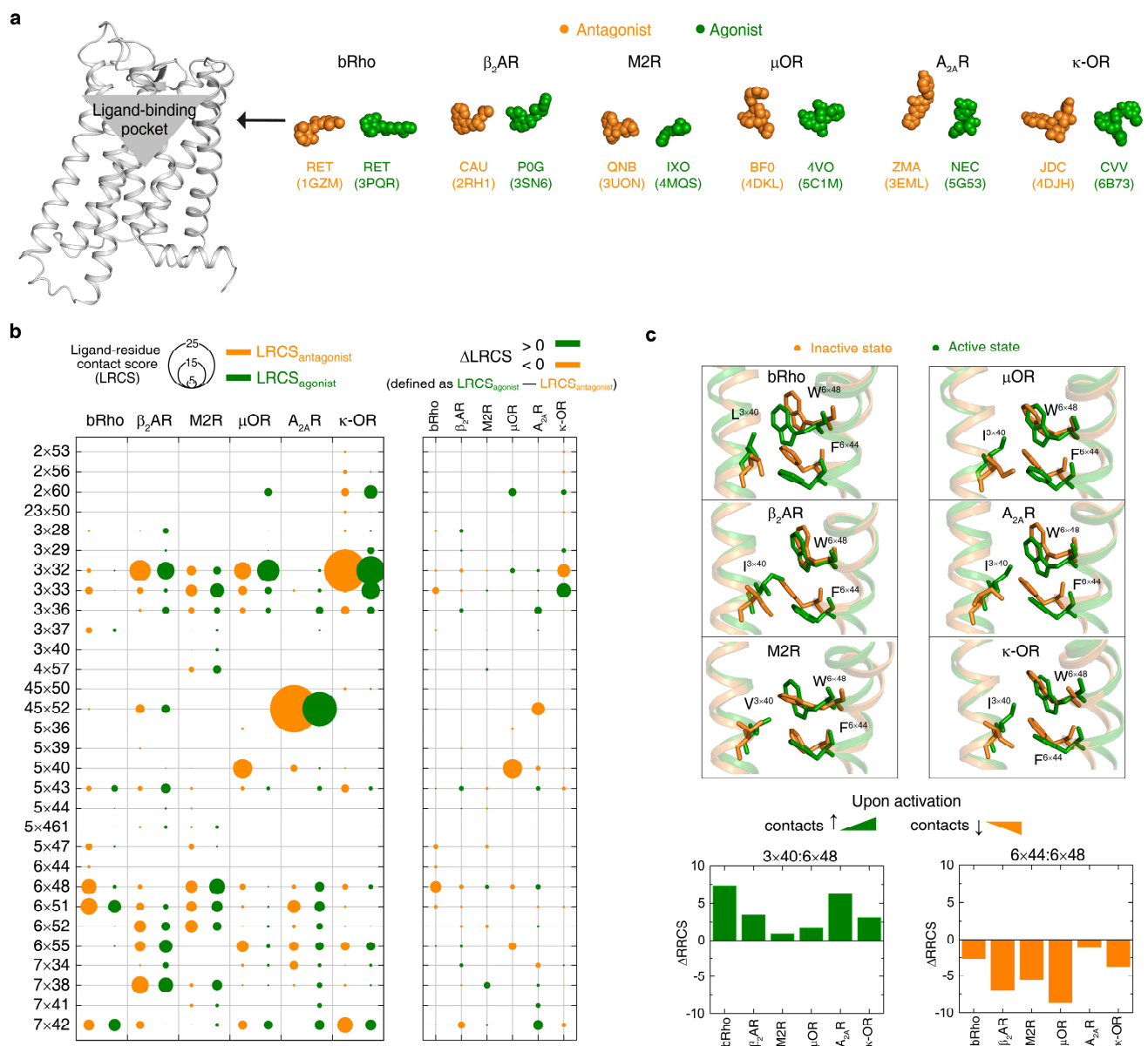
331 **Figure 2—figure supplement 1. Calculation of RRCS and Δ RRCS.** **a**, Workflow of RRCS
 332 calculation. **b**, Examples of RRCS and Δ RRCS calculation for two residues pairs. **c**, Statistics of
 333 residue contacts and contact types for six receptors (bRho, β_2 AR, M2R, μ OR, A_{2A}R and κ -OR) in their
 334 inactive and active states. Contact type describes physicochemical properties of two interacted amino
 335 acids that form a pair. The amino acids with hydrophobic side chains (one-letter code: A, V, I, L, M, P,
 336 F, Y, W) contribute to the majority of residue contacts, either within themselves (50.1%) or with other
 337 amino acids (37.8%).



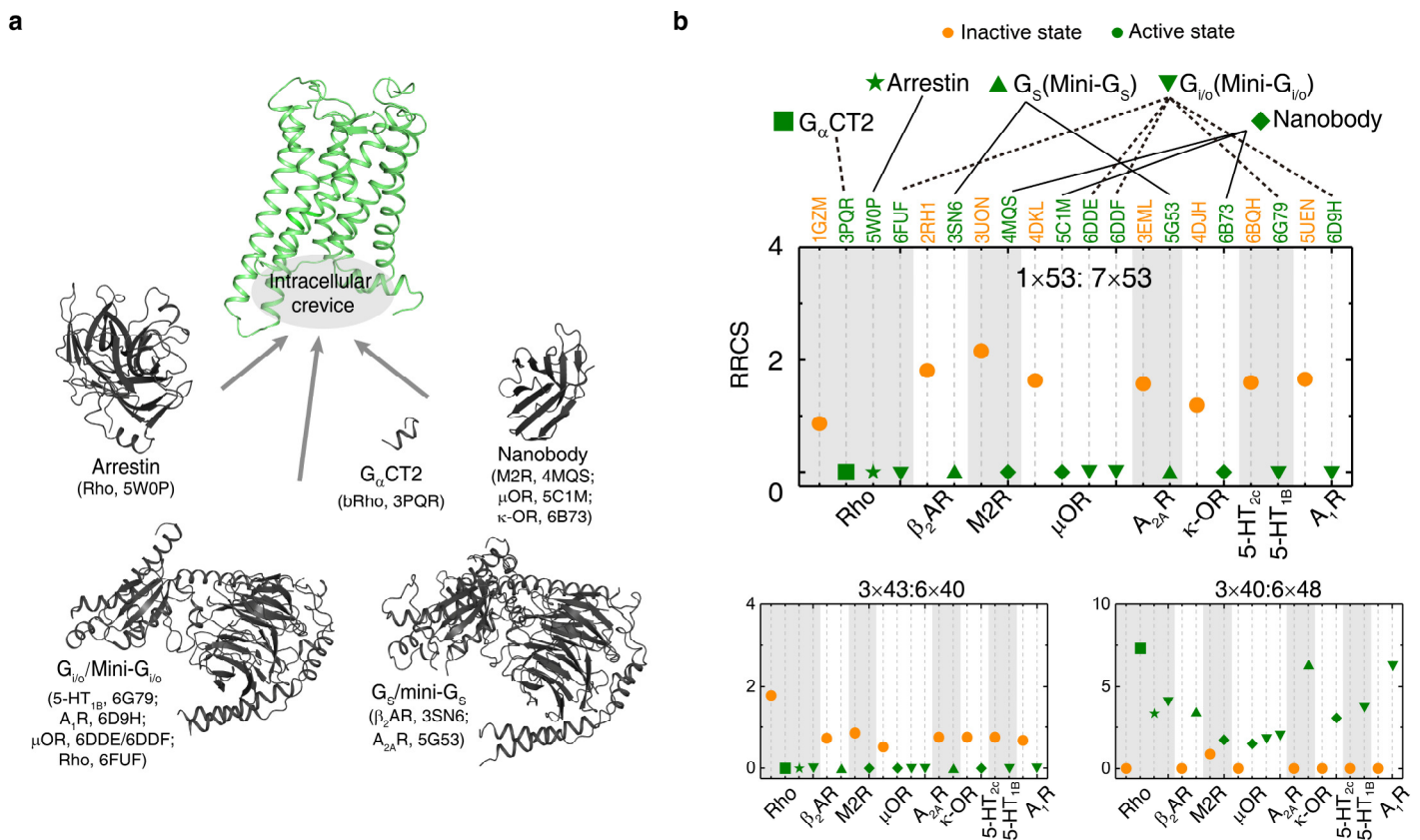
338 **Figure 3. Universal activation pathway of class A GPCRs.** Node represents structurally equivalent
 339 residue with the GPCRdb numbering³⁵ while the width of edge is proportional to the average Δ RRCS
 340 among six receptors (bRho, β_2 AR, M2R, μ OR, A_{2A}R and κ -OR). Four layers were qualitatively
 341 defined based on the topology of the pathway and their roles in activation: signal initiation (layer 1),
 342 signal propagation (layer 2), microswitches rewiring (layer 3) and G protein coupling (layer 4).

343 The following figure supplement is available for figure 3:

344 **Figure supplement 1.** Rearrangements of ligand-residue contacts in ligand-binding pocket are not
 345 conserved, reflecting diverse ligand recognition modes.



346
 347 **Figure 3—figure supplement 1. Rearrangements of ligand-residue contacts in ligand-binding**
 348 **pocket are not conserved, reflecting diverse ligand recognition modes. a,** Sphere representation of
 349 antagonist- and agonist-bound receptor crystal structures. **b,** Diverse LRCS and Δ LRCS reveal the
 350 repertoire of ligand recognition across class A GPCRs. The agonist or antagonist was treated as a
 351 single residue when calculating LRCS and Δ LRCS. As shown by the calculated Δ RRCS, no ligand-
 352 residue pair exhibits conserved rearrangements upon activation. **c,** Conserved conformational changes
 353 were only observed at the very bottom of ligand-binding pocket (6x48, 3x40 and 6x44).

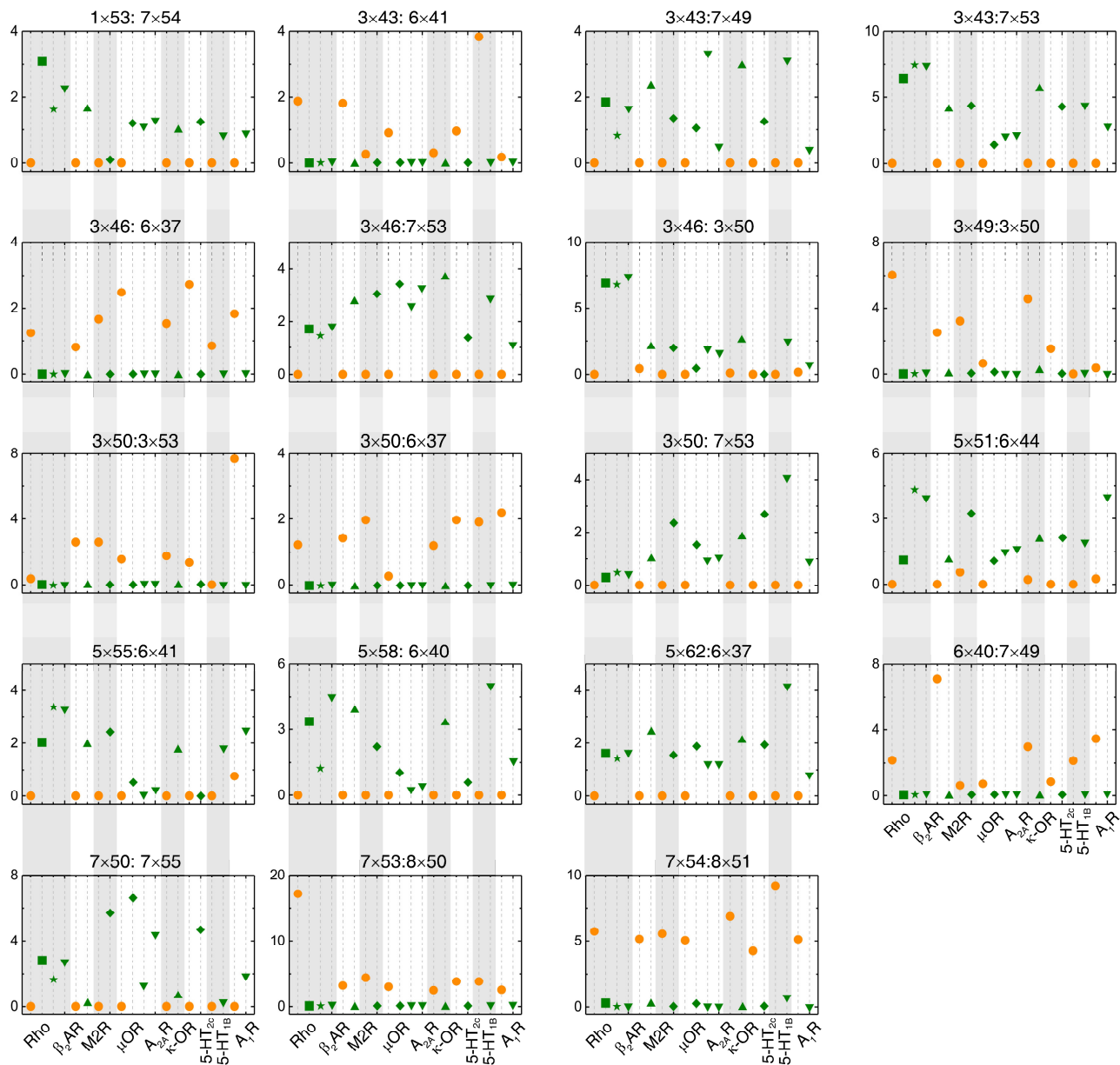


354 **Figure 4. The universal activation pathway is conserved, regardless of the subtypes of**
 355 **intracellular effectors. a**, Intracellular binding partners used in the active state structures. **b**,
 356 Comparison of RRCS for active (green) and inactive (orange) states of 8 receptors with different
 357 intracellular binding partners, including three recently solved cryo-EM structures of $G_{\beta\gamma}$ -bound
 358 receptors³⁸ (5-HT_{1B}, A₁R, μ OR) whose resolution were low (usually ≥ 3.8 Å for the GPCR part).
 359 Nevertheless, almost all conserved residue rearrangements in the pathway can be observed from these
 360 cryo-EM structures. Three of 34 residues pairs were shown here, see Figure 4—figure supplements 1
 361 and 2 for the remaining 31 residue pairs.

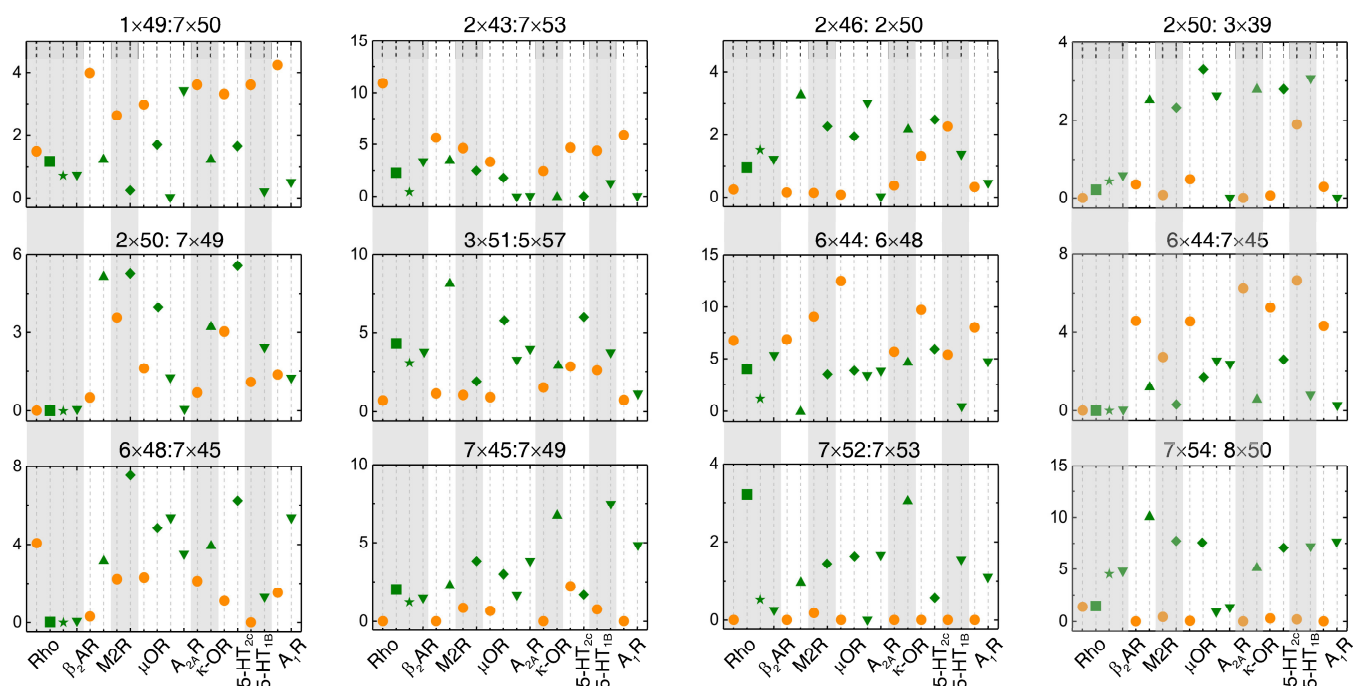
362 The following figure supplements are available for figure 4:

363 **Figure supplement 1.** The switching conformation change is conserved upon receptor activation,
 364 regardless of the subtypes of intracellular effectors.

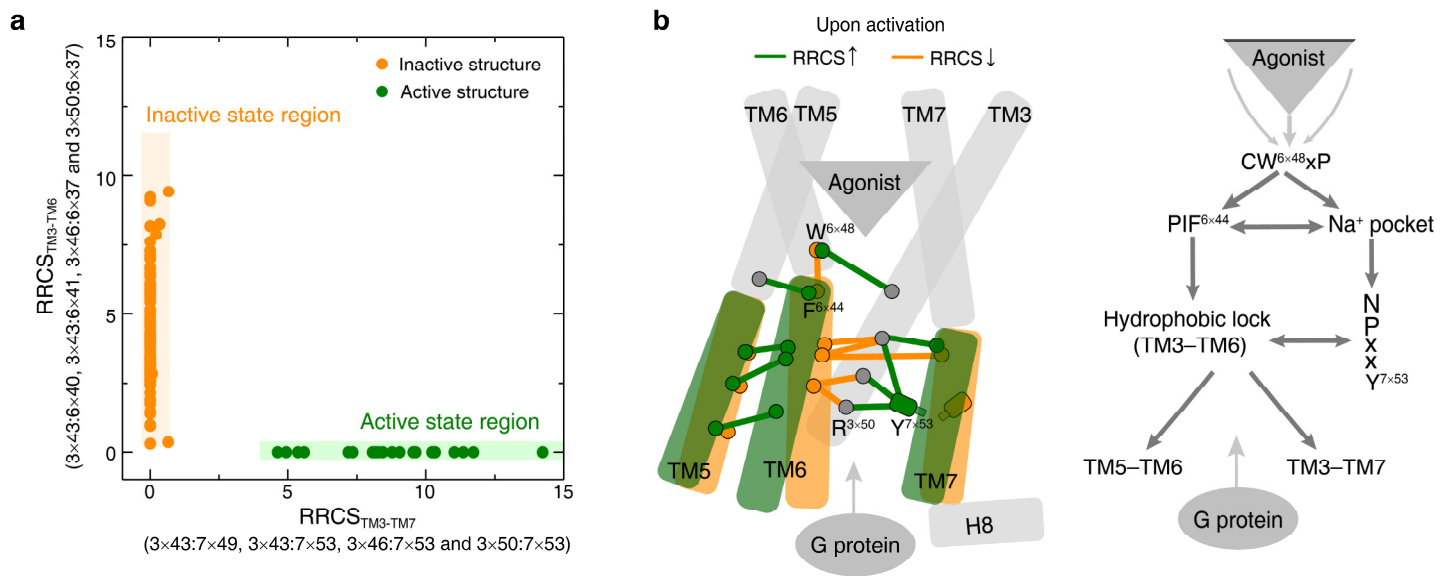
365 **Figure supplement 2.** The repacking conformation change is conserved upon receptor activation,
 366 regardless of the subtypes of intracellular effectors.



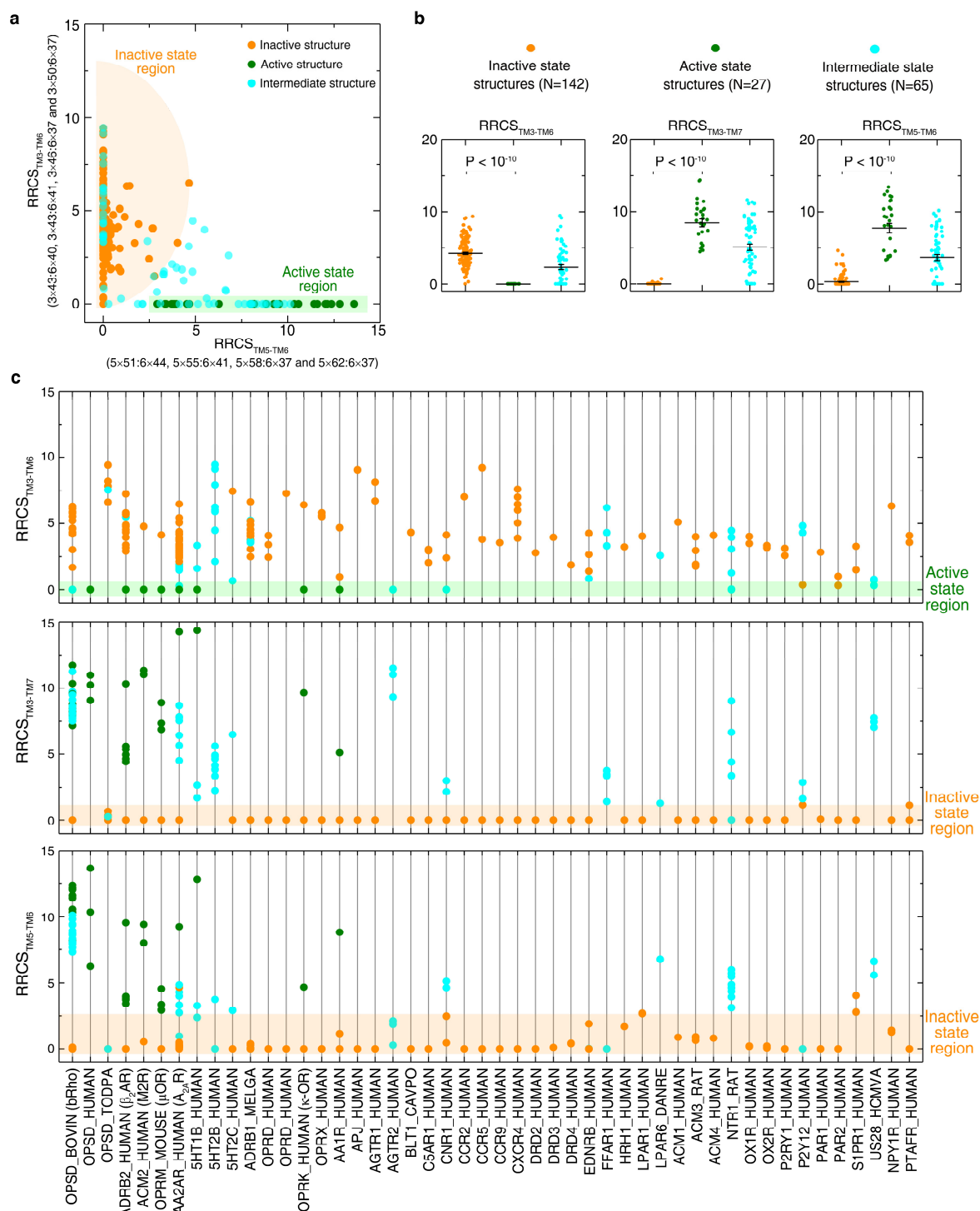
367 **Figure 4—figure supplement 1. The switching conformation change is conserved upon receptor**
 368 **activation, regardless of the subtypes of intracellular effectors.** Comparison of RRCS for active
 369 (green) and inactive (orange) states of 8 receptors with different intracellular binding partners,
 370 including three recently solved cryo-EM structures of G_{i/o}-bound receptors (5-HT_{1B}, A₁R, μ OR) whose
 371 resolution were low (usually ≥ 3.8 Å for the GPCR part)³⁸. Nevertheless, almost all conserved residue
 372 rearrangements in the pathway can be observed from these cryo-EM structures. Nineteen of 34
 373 residue pairs were shown here, see Figure 4 and Figure 4-figure supplement 2 for the remaining
 374 residue pairs.



375 **Figure 4—figure supplement 2. The repacking conformation change is conserved upon receptor**
 376 **activation, regardless of the subtypes of intracellular effectors.** Comparison of RRCS for active
 377 (green) and inactive (orange) states of 8 receptors with different intracellular binding partners,
 378 including three recently solved cryo-EM structures of $G_{i/o}$ -bound receptors (5-HT_{1B}, A₁R, μ OR) whose
 379 resolution were low (usually ≥ 3.8 Å for the GPCR part)³⁸. Nevertheless, almost all conserved residue
 380 rearrangements in the pathway can be observed from these cryo-EM structures. Twelve of 34 residues
 381 pairs were shown here, see Figure 4 and Figure 4-figure supplement 1 for the remaining residue pairs.



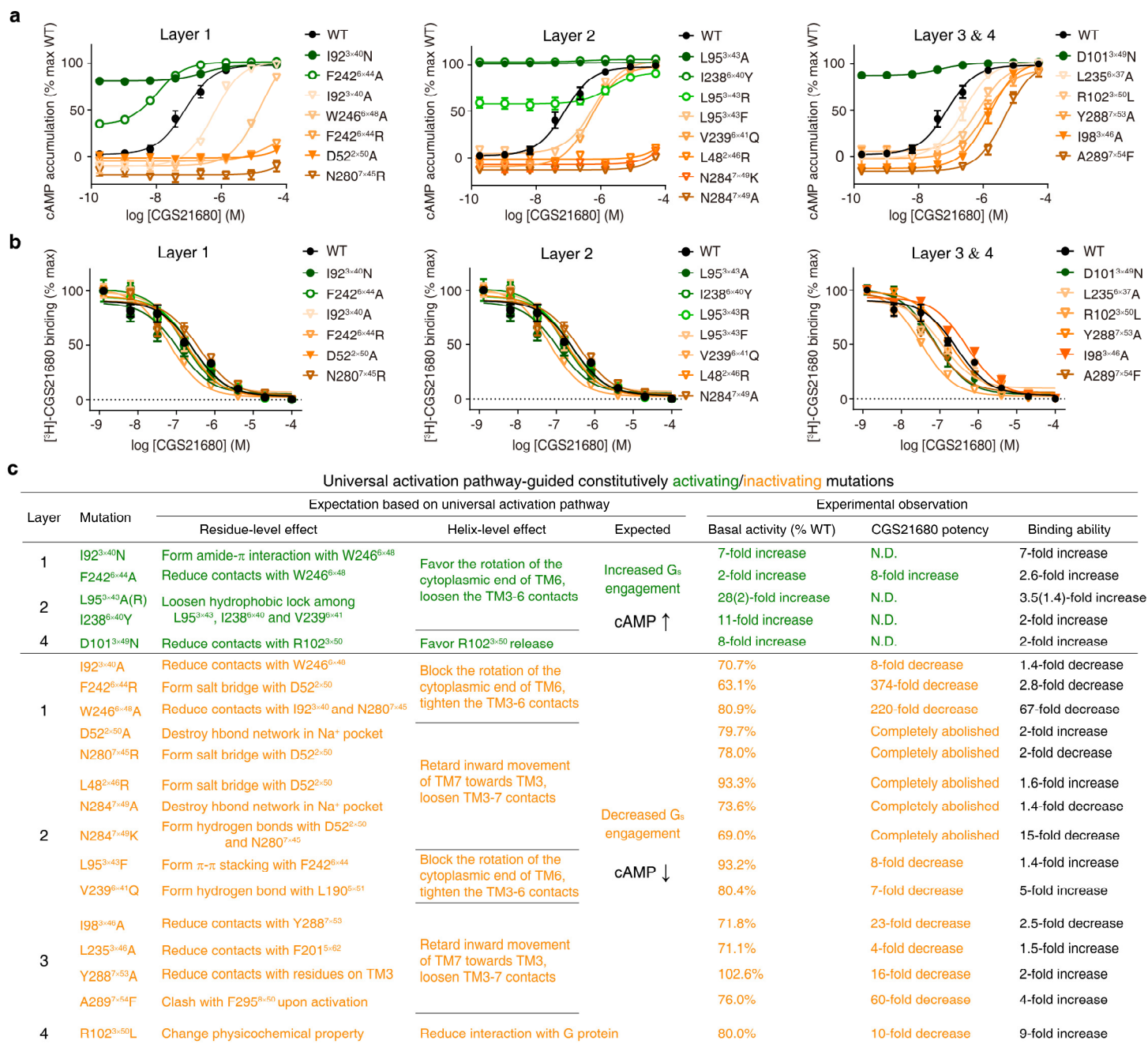
382 **Figure 5. Universal activation model of class A GPCRs reveals the major changes upon GPCR**
 383 **activation. a**, Active and inactive state structures form compact clusters in the 2D interhelical contact
 384 space: $RRCSTM3-TM7$ (X-axis) and $RRCSTM3-TM6$ (Y-axis). GPCR activation is best described by the
 385 outward movement of TM6 and inward movement of TM7, resulting in switch in the contacts of TM3
 386 from TM6 to TM7. **b**, Universal activation model for class A GPCRs. Residues are shown in circles,
 387 conserved contact rearrangements of residue pairs upon activation are denoted by lines.
 388 The following figure supplement is available for figure 5:
 389 **Figure supplement 1.** Global conformational change upon activation.



390

391 **Figure 5—figure supplement 1. Global conformational change upon activation. a,** Distinct
 392 clustering of inactive- and active-state structures in 2-dimensional interhelical contact space RRCS_{TM5-}
 393 _{TM6} vs. RRCS_{TM3-TM6}. **b,** The interhelical contacts comparison between inactive- and active-state
 394 structures. **c,** Receptor-specific interhelical contacts for all class A GPCR structures (inactive,

395 intermediate and active states are coloured in orange, cyan and green, respectively). These results
396 demonstrate that receptor activation involves the elimination of TM3-TM6 contacts, formation of
397 TM3-TM7 and TM5-TM6 contacts, reflecting the outward movement of the cytoplasmic end of TM6
398 away from TM3, the inward movement of TM7 towards TM3 and the repacking of TM5 and TM6.



399 **Figure 6. Experimental validation of the universal activation mechanism.** **a**, cAMP accumulation
 400 assay and **b**, radioligand binding assay, validated the universal activation pathway-guided design of
 401 CAMs/CIMs for A_{2A}R. WT, CAMs and CIMs are shown in black, green and orange, respectively. **c**,
 402 Mechanistic interpretation of universal activation pathway-guided CAMs/CIMs design. N.D.: basal
 403 activity was too high to determine an accurate EC₅₀ value.

404 The following data and figure supplement are available for figure 6:

405 **Source data 1.** Functional and ligand binding properties of A2AR mutations.

406 **Source data 2.** Analysis on the 14 unsuccessful predictions of A2AR CAMs/CIMs.

407 **Figure supplement 1.** Experimental validation of universal activation pathway-guided CAM/CIM
408 design.

409 **Figure 6—source data 1. Functional and ligand binding properties of A2AR mutations.**

Layer	Position	Mutation	Expression (%WT)	Binding assay IC ₅₀ (nM)	Function assay (cAMP accumulation)			
					Basal activity (% WT)	EC ₅₀ (nM)	Fold change in agonist potency	
WT			100	318.7 ± 41.2	100	78.4 ± 22.5		
CAM	1	6×44 F242A	92.0 ± 10.3	120.8 ± 17.8	196.5 ± 38.9	10.4 ± 1.4	7.5-fold increase	
		3×40 I92N	66.7 ± 6.4	43.8 ± 10.5	735.1 ± 131.8	N.D.*		
	2	3×43 L95A	96.7 ± 14.2	91.07 ± 53.0	2845.0 ± 738.6	N.D.*		
		3×43 L95R	42.3 ± 4.4	230.6 ± 57.1	224.8 ± 44.4	N.D.*	Constitutively active	
	4	6×40 I238Y	43.0 ± 2.1	159.8 ± 33.6	1074.9 ± 81.1	N.D.*		
CIM	1	3×49 D101N	41.7 ± 4.6	147.5 ± 99.4	840.6 ± 280.1	N.D.*		
		2×50 D52A	46.3 ± 1.7	154.6 ± 49.4	79.7 ± 7.8	N.D.†	Completely abolished	
		3×40 I92A	90.0 ± 8.6	440.3 ± 240.3	70.7 ± 2.2	593.6 ± 66.4	7.6-fold decrease	
		6×44 F242R	95.0 ± 2.7	894.0 ± 214.7	63.1 ± 12.6	29304.3 ± 12950.3	373.6-fold decrease	
		1	6×48 W246A	116.0 ± 12.5	21672.5 ± 5153.4	80.9 ± 9.2	17247.5 ± 3625.9	219.9-fold decrease
	7×45 N280R		87.7 ± 8.7	700.2 ± 225.7	78.0 ± 9.3	N.D.†	Completely abolished	
	2	2×46 L48R	63.7 ± 5.0	193.9 ± 50.6	93.3 ± 9.1	N.D.†	Completely abolished	
		3×43 L95F	98.7 ± 22.6	223.1 ± 79.3	93.2 ± 20.0	609.5 ± 42.1	7.8-fold decrease	
		6×41 V239Q	58.7 ± 4.9	60.1 ± 5.7	80.4 ± 12.8	515.7 ± 30.7	6.6-fold decrease	
		7×49 N284A	116.3 ± 17.0	459.1 ± 136.1	73.6 ± 11.1	N.D.†	Completely abolished	
		7×49 N284K	124.0 ± 24.6	5007.3 ± 1279.1	69.0 ± 4.3	N.D.†	Completely abolished	
		3×46 I98A	105.3 ± 15.1	818.2 ± 311.8	71.8 ± 4.3	1821.7 ± 513.3	23.2-fold decrease	
3	6×37 L235A	100.7 ± 11.1	211.3 ± 181.8	71.1 ± 8.5	298.6 ± 95.8	3.8-fold decrease		
	7×53 Y288A	63.3 ± 6.2	159.7 ± 50.2	102.6 ± 12.8	1262.2 ± 188.2	16.1-fold decrease		
	7×54 A289F	122.3 ± 13.9	75.6 ± 3.6	76.0 ± 10.0	4706.7 ± 644.1	60.0-fold decrease		
4	3×50 R102L	90.3 ± 4.8	33.9 ± 6.3	79.95 ± 29.6	789.1 ± 63.2	10.1-fold decrease		

410

411 * Basal activity was too high to determine an accurate EC₅₀ value.

412 † No stimulation of cAMP production was observed with 50 μM CGS21680.

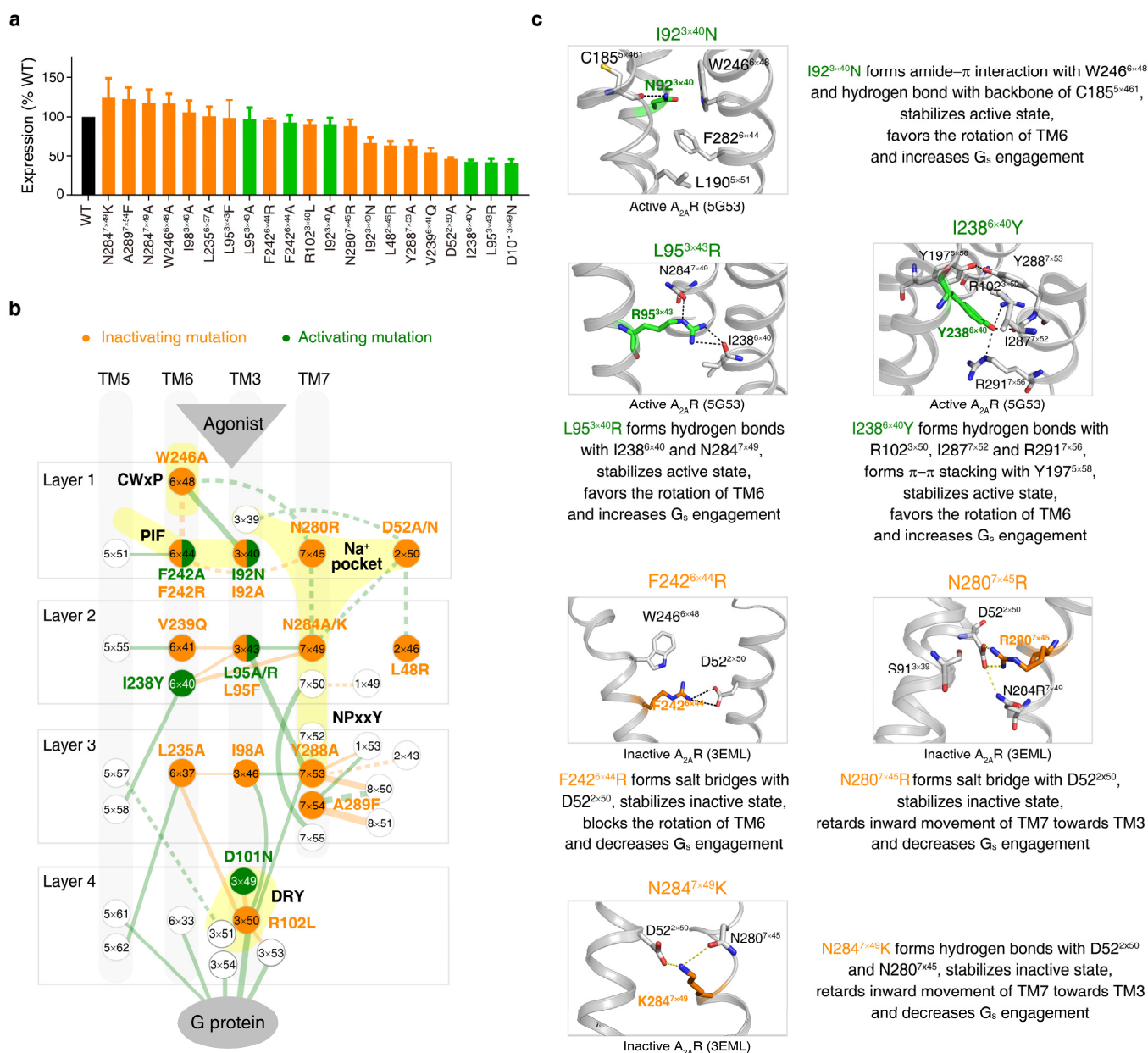
413 **Figure 6—source data 2. Analysis on the 14 unsuccessful predictions of A_{2A}R CAMs/CIMs.**

414 Δ Stability (>0 means destabilized; <0 means stabilized) is the change of receptor stability when a

415 mutation was introduced, calculated by Residue Scanning module in BioLuminate⁶¹. WT, wild-type.

Position	Mutation	Effect on inactive state (3EML)	Effect on active state (5G53)	Prediction	Experiment result	Discussion
Unsuccessful prediction of 9 CAMs						
3×46	I98N	Δ Stability >0	Δ Stability >0, H-bonds with F44 ^{2×42}	Stabilizes active state	Low expression	May affect receptor folding or trafficking.
3×46	I98E	Δ Stability >0	Δ Stability >0, salt bridge with R102 ^{3×50}	Stabilizes active state	CIM, >20-fold decrease in EC ₅₀	May affect G protein coupling interface
3×49	D101S	Δ Stability >0	Δ Stability <0, H-bonds with Y112 ^{34×53}	Breaks the restrains with R102 ^{3×50}	Close to WT	May affect G protein coupling interface
3×50	R102H	Δ Stability >0	Δ Stability >0, salt bridge with D101 ^{×49}	Stabilizes active state	Close to WT	May affect G protein coupling interface
3×51	Y103E	Δ Stability >0, salt bridge w/R107 ^{3×55}	Δ Stability >0, salt bridge with R199 ^{5×60}	Stabilizes TM5-TM6 contacts	Close to WT	May have indirect impact or no effect on TM6 rotation
6×40	I238Q	Δ Stability >0	Δ Stability >0, H-bonds with R102 ^{3×50} and R291 ^{7×56}	Stabilizes active state	Close to WT	Increases TM3-TM6 contacts, but may not affect the rotation of TM6
6×40	I238E	Δ Stability >0	Δ Stability >0, salt bridge with R102 ^{3×50}	Stabilizes active state	Close to WT	Increases TM3-TM6 contacts, but may not affect the rotation of TM6
6×40	I238A	Δ Stability >0, less hydrophobic contacts	Δ Stability >0, less hydrophobic contacts	Loosens TM3-TM6 contacts	Close to WT	Destabilizes both inactive and active states, but may not affect the rotation of TM6
7×45	N280S	Δ Stability >0	Δ Stability >0, H-bonds with W246 ^{6×48}	Stabilizes active state	Close to WT	Destabilizes both inactive and active states, but may not affect the rotation of TM6
Unsuccessful prediction of 5 CIMs						
3×40	I92Y	Δ Stability >0, stacking w/F242 ^{6×44}	Δ Stability >0, side chains rotate away from F242 ^{6×44}	Tightens TM3-6 contacts	Close to WT, slightly high basal activity	Makes the rotation of the cytoplasmic end of TM6 easier in active state
3×50	R102A	Δ Stability >0	Δ Stability >0, affect G protein coupling interface	Reduces interaction with G protein	Close to WT	A102 ^{3×50} doesn't affect G protein coupling for A _{2A} R
6×40	I238M	Δ Stability >0, more hydrophobic contacts	Δ Stability <0, more hydrophobic contacts	Tightens TM3-6 contacts	Close to WT	May stabilize the active state, but may not affect the rotation of TM6
6×44	F242T	Δ Stability >0	Δ Stability >0, may greatly affect signal initiation	May block the rotation of TM6	Close to WT	T242 ^{6×44} doesn't affect signal initiation for A _{2A} R
6×44	F242L	Δ Stability >0	Δ Stability >0, may greatly affect signal initiation	May block the rotation of TM6	Close to WT	L242 ^{6×44} doesn't affect signal initiation for A _{2A} R

416



417

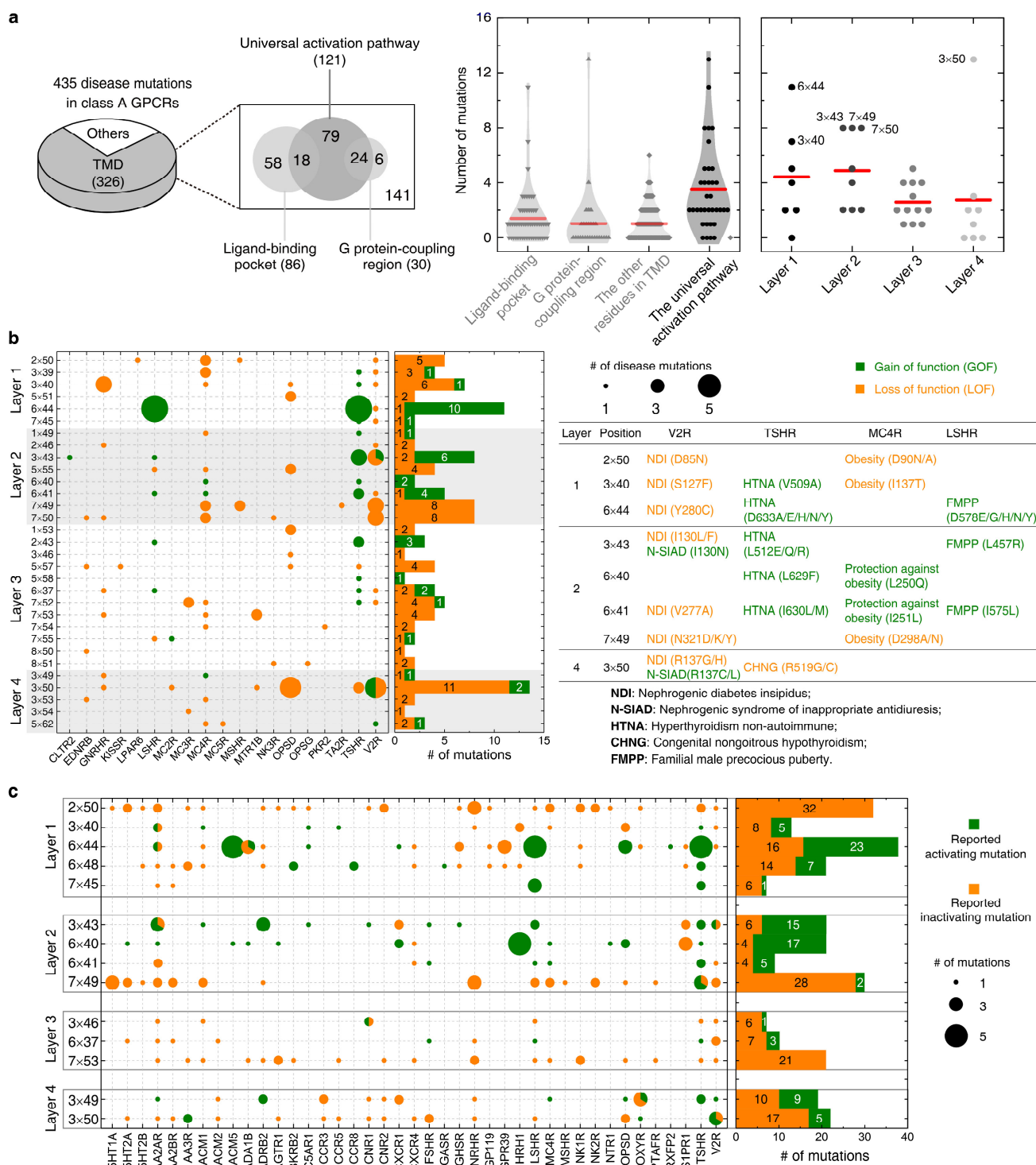
418 **Figure 6—figure supplement 1. Experimental validation of universal activation pathway-guided**

419 **CAM/CIM design. a**, Cell surface expression of the WT A_{2A}R and its mutants. WT, CAMs and CIMs

420 are coloured by black, orange and green, respectively. **b**, Mapping of validated CAMs/CIMs to the

421 universal activation pathway. **c**, The mechanisms of CAM/CIM design. CAMs and CIMs are in green

422 and orange, respectively.



423 **Figure 7. Importance of the universal activation pathway in pathophysiological and biological**
424 **context. a**, Comparison of disease-associated mutations in the universal activation pathway (further
425 decomposed into layers 1-4), ligand-binding pocket, G protein-coupling region and other regions. Red
426 line denotes the mean value. **b**, Mapping of disease-associated mutations in class A GPCRs to the

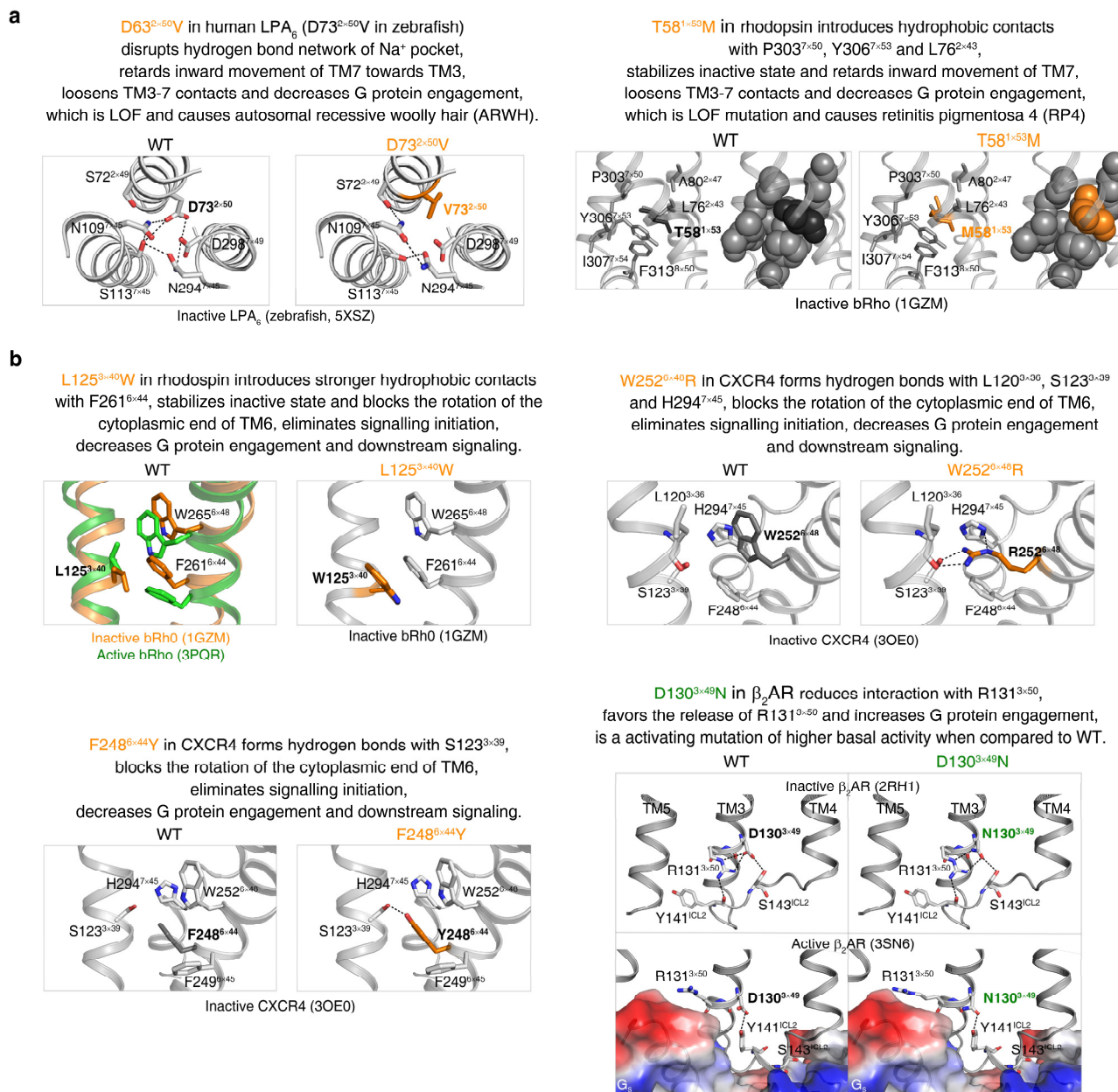
427 universal activation pathway. **c**, Key roles of the residues constituting the universal activation pathway
428 have been reported in numerous experimental studies on class A GPCRs. 272 CAMs/CIMs from 41
429 receptors were mined from the literature for the 14 hub residues (*i.e.*, residues that have more than one
430 edges in the pathway).

431 The following data and figure supplements are available for figure 7:

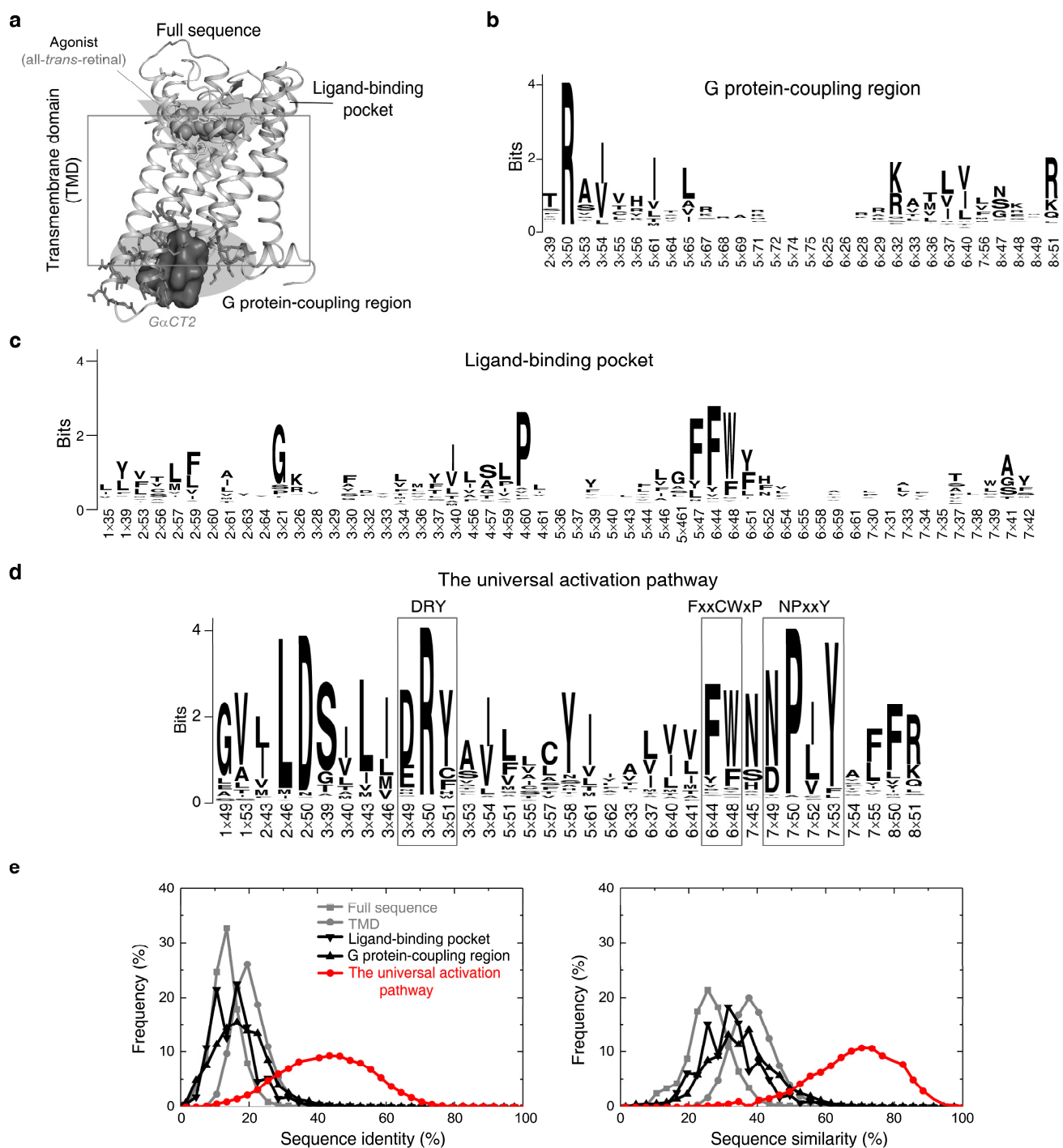
432 **Source data 1.** Constitutively activating/inactivating mutations for the 14 hub residues in the universal
433 activation pathway

434 **Figure supplement 1.** The universal activation pathway can be used to mechanistically interpret
435 disease-associated mutations and CAMs/CIMs.

436 **Figure supplement 2.** Residues in the universal activation pathway are more conserved than other
437 functional regions of GPCR.



438
 439 **Figure 7—figure supplement 1. The universal activation pathway can be used to mechanistically**
 440 **interpret disease-associated mutations and CAMs/CIMs. a, Pathway-guided mechanistic**
 441 **interpretations of two disease mutations. b, Pathway-guided mechanistic interpretations of four**
 442 **CAMs/CIMs.**



443
444 **Figure 7—figure supplement 2. Residues in the universal activation pathway are more conserved**
445 **than other functional regions of GPCR. a,** Illustration of different functional regions of GPCR. **b-d,**
446 **Sequence pattern of the G protein-coupling region (b), ligand-binding pocket (c) and the universal**
447 **activation pathway (d). e,** Distribution of sequence identity (left) and similarity (right) for functional
448 **regions across 286 non-olfactory class A receptors.**

449 **Materials and Methods**

450 **Glossary.**

451 Transmembrane domains (TMD): the core domain exists in all GPCRs, and consists of seven-
452 transmembrane helices (TM1–7) that are linked by three extracellular loops (ECL1-3) and three
453 intracellular loops (ICL1-3).

454 GPCRdb numbering scheme: a structure-based numbering system for GPCRs^{35, 62}, an improved
455 version of sequence-based Ballesteros–Weinstein numbering⁶³ that considers structural distortions
456 such as helical bulges or constrictions. The most conserved residue in a helix *n* is designated *n*×50,
457 while other residues on the helix are numbered relative to this position.

458 Node: a point in a network at which lines intersect, branch or terminate. In this case, nodes represent
459 amino acid residues.

460 Edge: a connection between the nodes in a network. In this case, an edge represents a residue-residue
461 contact.

462 Hub: a node with two or more edges in a network.

463 Constitutively activating mutation (CAM): a mutant that could increase the inherent basal activity of
464 the receptor by activating the G protein-signalling cascade in the absence of agonist.

465 Constitutively inactivating mutation (CIM): a mutant completely abolishes receptor signalling.

466 **GPCR structure data set.** As of October 1, 2018, there are 234 released structures of 45 class A
467 GPCRs with resolution better than 3.8 Å (Figure 1—Source data 1), which covers 71% (203 out of 286
468 receptors, including 158 receptors that have no structures but share >50% sequence similarity in the
469 TMD with the 45 structure-determined receptors) of class A GPCRs (Figure 1a). Based on the type of
470 bound ligand and effector, these structures could be classified into three states: inactive state
471 (antagonist or inverse agonist-bound, 142 structures from 38 receptors), active state (both agonist- and
472 G protein/G protein mimetic-bound, 27 structures from 8 receptors) and intermediate state (only
473 agonist-bound, 65 structures from 15 receptors). In this study, we primarily focused on conformational
474 comparison between inactive- and active- state structures, while also investigating the intermediate
475 state structures. In the structure data set, 7 receptors have both inactive and active structures: rhodopsin
476 (bRho), β₂-adrenergic receptor (β₂AR), M2 muscarinic receptor (M2R), μ-opioid receptor (μOR),
477 adenosine A_{2A} receptor (A_{2A}AR), κ-opioid receptor (κ-OR) and adenosine A_{1A} receptor (A_{1A}AR), the
478 active state structure of which was recently determined by cryo-EM. In addition, 32 receptors have
479 either inactive or active structures (Figure 1—Source data 1).

480 **Calculation of residue-residue contact score (RRCS).** We developed a much finer distance-based
481 method (than coarse-grained Boolean descriptors such as contact map and residues contact⁶⁴⁻⁶⁶),
482 namely residue-residue contact score (RRCS). For a pair of residues, RRCS is calculated by summing
483 up a plateau-linear-plateau form atomic contact score adopted from GPCR–CoINPocket^{34, 67-69} for each
484 possible inter-residue heavy atom pairs (Figure 2—figure supplement 1a). GPCR–CoINPocket is a
485 modified version of the hydrophobic term of ChemScore⁶⁴⁻⁶⁵ that has been successfully used to
486 describe hydrophobic contribution to binding free energy between ligand and protein. RRCS can
487 describe the strength of residue-residue contact quantitatively in a much more accurate manner than
488 Boolean descriptors^{8, 10}. For example, Boolean descriptors do not capture side chain repacking if the
489 backbone atoms of the two residues are close to each other (e.g., translocation of Y^{7×53} away from
490 residue at 2×43 upon GPCR activation) and local contacts involving adjacent residues (residues within

491 four/six amino acids in protein sequence) (e.g., disengagement between D/E^{3×49} and R^{3×50}), while both
492 cases can be well reflected by the change of RRCS (Figure 2c and Figure 2—figure supplement 1b).

493 All RRCS data can be found in Figure 2—Source data 1. The computational details are listed as below:

494 (i) For the residue pairs between adjacent residues that are within four amino acids in protein sequence,
495 only side chain heavy atom pairs were considered, atom pairs involving in backbone atoms (Ca, C, O,
496 N) were excluded, since the latter seldom change during GPCR activation. For other residue pairs, all
497 possible heavy atom pairs (including backbone atoms) were included when calculating RRCS.

498 (ii) Atomic contact scores are solely based on interatomic distance, and they were treated equally
499 without weighting factors such as atom type or contact orientation. In principle, weighting of atomic
500 contact by atom type and/or orientation would improve residue-residue contact score. However,
501 parameterization of atom type or contact orientation is relatively arbitrary, subjective and complicated,
502 especially considering the lipid bilayer environment surrounding GPCRs. Our preliminary study for
503 twelve structures from six receptors (bRho, β_2 AR, M2R, μ OR, A_{2A}R and κ -OR) revealed that amino
504 acids with hydrophobic side chains (one-letter code: A, V, I, L, M, P, F, Y, W) contribute to the
505 majority (~88%) of residue pairs. Meanwhile, ionic lock opening of well-known motif DRY upon
506 receptor activation can be adequately reflected by RRCS change between D/E^{3×49} and R^{3×50}. These
507 results suggest that interatomic distance-dependent residue pair contact score may represent an
508 acceptable approximation of actual (either hydrophobic or charge-charge) interaction energies³⁴ and is
509 accurate enough for identifying conserved rearrangements of residue contacts upon receptor activation.

510 (iii) The quality of structures is extremely important for RRCS calculation. We adopted two criteria to
511 exclude unreliable structures and residues: (a) crystal structures whose resolution is ≥ 3.8 Å. Structures
512 in this category are: 5DGY (7.70 Å), 2I37 (4.20 Å), 2I36 (4.10 Å), 5TE5 (4.00 Å), 4GBR (4.00 Å),
513 5NJ6 (4.00 Å), 5V54 (3.90 Å), 2I35 (3.80 Å), 5D5B (3.80 Å), 4XT3 (3.80 Å); (b) residues whose
514 residue-based real-space R-value (RSR⁷⁰) is greater than 0.35. RSR is measure of how well ‘observed’
515 and calculated electron densities agree for a residue. RSR ranges from 0 (perfect match) to 1 (no
516 match); RSR greater than 0.4 indicates a poor fit⁷¹. Here we adopted a stricter cut-off, 0.35. Among the
517 234 class A GPCR structures, 156 have available RSR information⁷² (<http://eds.bmc.uu.se>), with 8.8%
518 residues have RSR >0.35 and they are omitted in our analysis. For the 35 residues that constitute the
519 universal activation pathway, 255 out of 5460 RSR data points (~4.7%, lower than 8.8% for all
520 residues) were omitted for having RSR values >0.35.

521 (iv) For structures with multiple chains, RRCS were the average over all chains. For residues with
522 multiple alternative conformations, RRCS is the sum of individual values multiplied by the weighting
523 factor: occupancy value extracted from PDB files. Small molecule/peptide ligand, or intracellular
524 binding partner (G protein or its mimetic) was treated as a single residue.

525 (v) For the family-wide comparison of conformational changes upon activation, structurally equivalent
526 residues are numbered by GPCRdb numbering scheme^{35, 62}. Of the 35 residues in the universal
527 activation pathway, their GPCRdb numbering in all structures is almost identical to the Ballesteros–
528 Weinstein numbering⁶³, the exceptions are residues at 6×37, 6×41 and 6×44 for five receptors:
529 FFAR1, P2Y₁, P2Y₁₂, F2R and PAR2, which are all from the delta branch of class A family.

530 **Identification of conserved rearrangements of residue contacts upon activation.** Using RRCS,
531 structural information of TMD and helix 8 in each structure can be decomposed into 400~500 residue
532 pairs with positive RRCS. Δ RRCS, defined as RRCS_{active} – RRCS_{inactive}, reflects the change of RRCS
533 for a residue pair from inactive- to active- state (Figure 2b-d and Figure 2—figure supplement 1b). To
534 identify residue pairs with conserved conformational rearrangements upon activation across class A

535 GPCRs, two rounds of selections (Figure 2d and Figure 2—Source data 1) were performed: (i)
536 identification of conserved rearrangements of residue contacts upon activation for six receptors (bRho,
537 β_2 AR, M2R, μ OR, A_{2A}AR and κ -OR), *i.e.*, equivalent residue pairs show a similar and substantial
538 change in RRCS between the active and inactive state structure of each of the six receptors (the same
539 sign of Δ RRCS and $|\Delta$ RRCS| > 0.2 for all receptors) and (ii) family-wide RRCS comparison between
540 the 142 inactive and 27 active state structures to identify residues pairs of statistically significant
541 different ($P < 0.001$; two sample *t*-test) RRCS upon activation.

542 Round 1. Identification of conserved rearrangements of residue contacts. Six receptors with available
543 inactive- and active- state structures were analysed using Δ RRCS to identify residue pairs that share
544 similar conformational changes. Twelve representative crystal structures (high-resolution, no mutation
545 or one mutation in TMD without affecting receptor signalling) were chosen in this stage: 6 inactive
546 state structures (PDB codes 1GZM for bRho, 2RH1 for β_2 AR, 3UON for M2R, 4DKL for μ OR, 3EML
547 for A_{2A}AR and 4DJH for κ -OR) and 6 active state structures (3PQR for bRho, 3SN6 for β_2 AR, 4MQS
548 for M2R, 5C1M for μ OR, 5G53 for A_{2A}AR and 6B73 for κ -OR) (Figure 2d, Figure 2—figure
549 supplement 1c and Figure 2—Source data 1). Each receptor has approximately 600 residues pairs that
550 have positive RRCS. Roughly one quarter are newly formed during receptor activation ($RRCS_{\text{inactive}} = 0$
551 & $RRCS_{\text{active}} > 0$); another quarter lose their contacts upon receptor activation ($RRCS_{\text{inactive}} > 0$ &
552 $RRCS_{\text{active}} = 0$); and the remaining appear in both the inactive- or active- state structures
553 ($RRCS_{\text{inactive}} > 0$ & $RRCS_{\text{active}} > 0$), the contact rearrangement of which can only be reflected by Δ RRCS,
554 but not Boolean descriptors.

555 To identify residue pairs that share conserved rearrangements of residue contacts upon activation, two
556 steps are performed to qualify residue pairs for the next round. Firstly, residue pairs with same sign of
557 Δ RRCS and $|\Delta$ RRCS| > 0.2 for all six receptors were identified. There are 32 intra-receptor residues
558 pairs (1×49:7×50, 1×53:7×53, 1×53:7×54, 2×37:2×40, 2×42:4×45, 2×43:7×53, 2×45:4×50,
559 2×46:2×50, 2×50:3×39, 2×57:7×42, 3×40:6×48, 3×43:6×40, 3×43:6×41, 3×43:7×49,
560 3×43:7×53, 3×46:6×37, 3×46:7×53, 3×49:3×50, 3×50:3×53, 3×50:6×37, 350:7×53,
561 3×51:5×57, 5×51:6×44, 5×58:6×40, 5×62:6×37, 6×40:7×49, 6×44:6×48, 7×50:7×55,
562 7×52:7×53, 7×53:8×50, 7×54:8×50 and 7×54:8×51) and 5 receptor-G protein/its mimetic residue
563 pairs (3×50:G protein, 3×53:G protein, 3×54:G protein, 5×61:G protein and 6×33:G protein) that
564 meet this criterion. Secondly, we also investigated residue pairs with Δ RRCS that are conserved in five
565 receptors (*i.e.*, with one receptor as exception). Considering there is no Na⁺ pocket for rhodopsin, 3
566 residue pairs (2×50:7×49, 6×44:7×45, 6×48:7×45) around Na⁺ pocket were analysed for five
567 receptors but not bRho. Additionally, 3 residue pairs have 0 (3×46:3×50, 5×55:6×41) or negative
568 (7×45:7×49) Δ RRCS for κ -OR but positive Δ RRCS for the other five receptors. As for 3×46:3×50,
569 nanobody-stabilized active structures (β_2 AR: 3P0G, 4LDO, 4LDL, 4LDE, 4QKX; and μ OR: 5C1M)
570 generally have lower contact scores (<0.4) compared with G protein-bound active-state structures
571 (2.17 for 3SN6 of β_2 AR, 2.57 for 5G53 of A_{2A}AR and 6.93 for 3PQR of bRho). For these residue pairs,
572 we added newly determined G_i-bound active receptors A_{1A}AR and 5-HT_{1B} and found they have positive
573 Δ RRCS, like other five receptors (Figure 4—figure supplements 1 and 2). Thus, these three residue
574 pairs (3×46:3×50, 5×55:6×41 and 7×45:7×49) were retained. Totally, 6 residue pairs with
575 conserved Δ RRCS in five receptors were rescued. Taken together, 38 intra-receptor residue pairs and 5
576 receptor-G protein/its mimetic residue pairs were identified to have conserved rearrangements of
577 residue contacts upon activation.

578 Round 2. Family-wide conservation analysis of residue contact pattern. To investigate the conservation
579 of residue contact pattern for the 38 intra-receptor residue pairs across these functionally diverse
580 receptors, two-tailed unpaired *t*-test between inactive state (142 inactive structures from 38 receptors)

581 and active state (27 active structures from 8 receptors) groups were performed (Figure 2d and Figure
582 2—Source data 2). Thirty one residue pairs have significantly different RRCS between inactive- and
583 active-state ($P < 10^{-5}$). As rhodopsin lacks Na^+ pocket, all rhodopsin structures were neglected in the
584 analysis of 3 residue pairs around Na^+ pocket (2×50:7×49, 6×44:7×45 and 6×48:7×45), which have
585 good P value ($< 10^{-3}$) for these non-rhodopsin class A GPCRs. 4 residue pairs were filtered out in this
586 round due to their poor P value, *i.e.*, there are no statistically significant difference in RRCS between
587 inactive and active states ($P=0.01$ for 2×37:2×40, 0.96 for 2×42:4×45, 0.02 for 2×45:4×50 and
588 0.014 for 2×57:7×42).

589 Finally, 34 intra-receptor residue pairs (Figure 2d, Figure 4—figure supplements 1 and 2) and 5
590 receptor-G protein residue pairs were identified with conserved rearrangements of residue contacts
591 upon activation, including all six residues pairs identified by the previous RC approaches⁸.

592 **Sequence analysis of class A GPCRs.** The alignment of 286 non-olfactory, class A human GPCRs
593 were obtained from the GPCRdb^{35, 62}. The distribution of sequence similarity/identity across class A
594 GPCRs were extracted from the sequence similarity/identity matrix for different structural regions by
595 using “Similarity matrix” tool in GPCRdb. The sequence conservation score (Figure 1—figure
596 supplement 1) for all residue positions across 286 non-olfactory class A GPCRs were evaluated by the
597 Protein Residue Conservation Prediction⁵⁶ tool with scoring method “property entropy”⁵⁷. Sequence
598 conservation analysis (Figure 7—figure supplement 2) were visualized by WebLogo3⁷³ with sequence
599 alignment files from GPCRdb as the input.

600 **CAM/CIM in class A GPCRs.** For the 14 hub residues in the universal activation pathway, we
601 collected the functional mutation data from literature and GPCRdb^{35, 62}. Mutations with “more than
602 two fold-increase in basal activity/constitutively active” or “abolished effect” compared to the wild-
603 type receptor were selected. Together, 272 mutations from 41 class A GPCRs on the 14 hub residues
604 were collected, including the mutations we designed and validated in this work (Figure 7—source data
605 1).

606 **Disease-associated mutations in class A GPCRs.** To reveal the relationship between disease-
607 associated mutations and associated phenotypes of different transmembrane regions⁷⁴⁻⁷⁷, we collected
608 disease-associated mutation information for all 286 non-olfactory class A GPCRs by database
609 integration and literature investigation. Four commonly used databases (UniProt⁵⁸, OMIM⁵⁹,
610 Ensembl⁶⁰ and GPCRdb⁵⁴⁻⁵⁵) were first filtered by disease mutations and then merged. Totally 435
611 disease mutations from 61 class A GPCRs were collected (Figure 1—Source data 2).

612 **Pathway-guided CAM/CIM design in A_{2A}R.** We designed mutations for a prototypical receptor
613 A_{2A}R, guided by the universal activation pathway, aiming to get constitutively active/inactive receptor.
614 Mutations that can either stabilize active or inactive state structures of A_{2A}R or promote/block the
615 conformational change upon activation were designed (Figure 6c and Figure 6—figure supplement 1)
616 and tested by functional cAMP accumulation assays. The inactive state structure 3EML and active
617 state structure 5G53 were used. *In silico* mutagenesis was performed by Residue Scanning module in
618 BioLuminate⁶¹. Sidechain prediction with backbone sampling and a cut-off value of 6Å were applied
619 during the scanning. Δ Stability is the change of receptor stability when introducing a mutation. We
620 filtered the mutations by one of the following criteria: (i) Δ Stability in active and inactive structures
621 have opposite sign; or (ii) Δ Stability in active and inactive structures have the same sign, but
622 favourable interactions such as hydrogen bonds, salt bridge or pi-pi stacking exist in only one structure
623 that can promote/block the conformational change upon activation. Totally, 15 and 20 mutations were
624 predicted to be CAMs and CIMs, respectively. (Figure 6c and Figure 6—figure supplement 1).

625 **cAMP accumulation assay.** The desired mutations were introduced into amino-terminally Flag® tag-
626 labeled human A_{2A}R in the pcDNA3.1 vector (Invitrogen, Carlsbad, CA, USA). This construct
627 displayed equivalent pharmacological features to that of untagged human receptor based on
628 radioligand binding and cAMP assays⁷⁸. The mutants were constructed by PCR-based site-directed
629 mutagenesis (Muta-direct™ kit, Beijing SBS Genetech Co., Ltd., China). Sequences of receptor
630 clones were confirmed by DNA sequencing. HEK-293 cells were seeded onto 6-well cell culture plates.
631 After overnight culture, the cells were transiently transfected with WT or mutant DNA using
632 Lipofectamine 2000 transfection reagent (Invitrogen). After 24 h, the transfected cells were seeded
633 onto 384-well plates (3,000 cells per well). cAMP accumulation was measured using the LANCE
634 cAMP kit (PerkinElmer, Boston, MA, USA) according to the manufacturer's instructions. Briefly,
635 transfected cells were incubated for 40 min in assay buffer (DMEM, 1 mM 3-isobutyl-1-
636 methylxanthine) with different concentrations of agonist [CGS21680 (179 pM to 50 μM)]. The
637 reactions were stopped by addition of lysis buffer containing LANCE reagents. Plates were then
638 incubated for 60 min at room temperature and time-resolved FRET signals were measured at 625 nm
639 and 665 nm by an EnVision multilabel plate reader (PerkinElmer). The cAMP response is depicted
640 relative to the maximal response of CGS21680 (100%) at the WT A_{2A}R.

641 **CGS21680 binding assay.** CGS21680 (a specific adenosine A_{2A} subtype receptor agonist) binding
642 was analyzed using plasma membranes prepared from HEK-293 cells transiently expressing WT and
643 mutant A_{2A}Rs. Approximately 1.2×10^8 transfected HEK-293 cells were harvested, suspended in 10
644 ml ice-cold membrane buffer (50 mM Tris-HCl, pH 7.4) and centrifuged for 5 min at 700 *g*. The
645 resulting pellet was resuspended in ice-cold membrane buffer, homogenized by Dounce Homogenizer
646 (Wheaton, Millville, NJ, USA) and centrifuged for 20 min at 50,000 *g*. The pellet was resuspended,
647 homogenized, centrifuged again and the precipitate containing the plasma membranes was then
648 suspended in the membrane buffer containing protease inhibitor (Sigma-Aldrich, St. Louis, MO, USA)
649 and stored at -80°C. Protein concentration was determined using a protein BCA assay kit (Pierce
650 Biotechnology, Pittsburgh, PA, USA). For homogeneous binding, cell membrane homogenates (10 μg
651 protein per well) were incubated in membrane binding buffer (50 mM Tris-HCl, 10 mM NaCl, 0.1 mM
652 EDTA, pH 7.4) with constant concentration of [³H]-CGS21680 (1 nM, PerkinElmer) and serial
653 dilutions of unlabeled CGS21680 (0.26 nM to 100 μM) at room temperature for 3 h. Nonspecific
654 binding was determined in the presence of 100 μM CGS21680. Following incubation, the samples
655 were filtered rapidly in vacuum through glass fiber filter plates (PerkinElmer). After soaking and
656 rinsing 4 times with ice-cold PBS, the filters were dried and counted for radioactivity in a MicroBeta2
657 scintillation counter (PerkinElmer).

658 **Surface expression of A_{2A}Rs.** HEK-293 cells were seeded into 6-well plate and incubated overnight.
659 After transient transfection with WT or mutant plasmids for 24 h, the cells were collected and blocked
660 with 5% BSA in PBS at room temperature for 15 min and incubated with primary anti-Flag antibody
661 (1:100, Sigma-Aldrich) at room temperature for 1 h. The cells were then washed three times with PBS
662 containing 1% BSA followed by 1 h incubation with anti-rabbit Alexa-488-conjugated secondary
663 antibody (1:1000, Cell Signaling Technology, Danvers, MA, USA) at 4°C in the dark. After three
664 washes, the cells were resuspended in 200 μl of PBS containing 1% BSA for detection in a NovoCyte
665 flow cytometer (ACEA Biosciences, San Diego, CA, USA) utilizing laser excitation and emission
666 wavelengths of 488 nm and 519 nm, respectively. For each assay point, approximately 15,000 cellular
667 events were collected, and the total fluorescence intensity of positive expression cell population was
668 calculated.

669 **Data and materials availability:** The open source code is available at GitHub
670 (<https://github.com/zhaolabSHT/RRCS>). For availability of codes that were developed in-house, please
671 contacts the corresponding authors. All data is available in the main text or the source data.

672 **Acknowledgments:** This work was partially supported by National Key R&D Program of China
673 grants 2016YFC0905900 (S.Z.) and 2018YFA0507000 (S.Z. and M.-W.W.), National Mega R&D
674 Program for Drug Discovery grants 2018ZX09711002-002-005 (D.H.Y.) and 2018ZX09735-001 (M.-
675 W.W), National Natural Science Foundation of China grants 21704064 (Q.Z.), 81573479 (D.H.Y.) and
676 81773792 (D.H.Y.), Shanghai Science & Technology Development Fund grants 16ZR1448500 (S.Z.)
677 and 16ZR1407100 (A.T.D.), Young Talent Program of Shanghai (S.Z.), Novo Nordisk-CAS Research
678 Fund grant NNCAS-2017-1-CC (D.H.Y.), the Medical Research Council MC_U105185859 (M.M.B.),
679 and annual overhead support from ShanghaiTech University and Chinese Academy of Sciences. We
680 thank A. Sali, M.A. Hanson and A.J. Venkatakrishnan for valuable discussions, Y.M. Xu for technical
681 assistance, and A.P. IJzerman for providing the WT A_{2A}R plasmid.

682 **Authors contributions:** Q.Z. and S.Z. conceived the project; M.-W.W. and M.M.B. expanded the
683 scope of the project. Q.Z. performed computational studies. Q.Z., D.H.Y., S.Z. and M.M.B. designed
684 the mutagenesis experiments. M.W. helped with data collection and initial mutagenesis study. Y.G.
685 wrote the code for RRCS calculation. W.J.G., L.Z., X.Q.C., A.T.D. and D.H.Y. conducted
686 mutagenesis and pharmacology experiments with the supervision of M.-W.W. E.S., Z.-J.L. and R.C.S.
687 provided academic support or technical inputs to the project. Q.Z., D.H.Y., M.M.B., M-W.W. and S.Z.
688 interpreted the data and wrote the manuscript. S.Z. and M.-W.W. managed the entire project.

689 **Competing interests:** The authors declare no competing interests.

690

691 References

- 692 1. Deupi, X.; Standfuss, J., Structural insights into agonist-induced activation of G-protein-coupled receptors. *Curr Opin Struct Biol* **2011**, *21* (4), 541-51. <https://doi.org/10.1016/j.sbi.2011.06.002>.
- 693
- 694 2. Venkatakrishnan, A. J.; Deupi, X.; Lebon, G.; Tate, C. G.; Schertler, G. F.; Babu, M. M., Molecular signatures of
695 G-protein-coupled receptors. *Nature* **2013**, *494* (7436), 185-94. <https://doi.org/10.1038/nature11896>.
- 696 3. Katritch, V.; Cherezov, V.; Stevens, R. C., Structure-function of the G protein-coupled receptor superfamily. *Annu*
697 *Rev Pharmacol Toxicol* **2013**, *53*, 531-56. <https://doi.org/10.1146/annurev-pharmtox-032112-135923>.
- 698 4. Erlandson, S. C.; McMahon, C.; Kruse, A. C., Structural Basis for G Protein-Coupled Receptor Signaling. *Annu*
699 *Rev Biophys* **2018**. <https://doi.org/10.1146/annurev-biophys-070317-032931>.
- 700 5. Weis, W. I.; Kobilka, B. K., The Molecular Basis of G Protein-Coupled Receptor Activation. *Annual review of*
701 *biochemistry* **2018**, *87*, 897-919. <https://doi.org/10.1146/annurev-biochem-060614-033910>.
- 702 6. Ghosh, E.; Kumari, P.; Jaiman, D.; Shukla, A. K., Methodological advances: the unsung heroes of the GPCR
703 structural revolution. *Nat Rev Mol Cell Biol* **2015**, *16* (2), 69-81. <https://doi.org/10.1038/nrm3933>.
- 704 7. Cooke, R. M.; Brown, A. J.; Marshall, F. H.; Mason, J. S., Structures of G protein-coupled receptors reveal new
705 opportunities for drug discovery. *Drug Discov Today* **2015**, *20* (11), 1355-64. <https://doi.org/10.1016/j.drudis.2015.08.003>.
- 706 8. Venkatakrishnan, A. J.; Deupi, X.; Lebon, G.; Heydenreich, F. M.; Flock, T.; Miljus, T.; Balaji, S.; Bouvier, M.;
707 Veprintsev, D. B.; Tate, C. G.; Schertler, G. F.; Babu, M. M., Diverse activation pathways in class A GPCRs converge near
708 the G-protein-coupling region. *Nature* **2016**, *536* (7617), 484-7. <https://doi.org/10.1038/nature19107>.
- 709 9. Wootten, D.; Christopoulos, A.; Marti-Solano, M.; Babu, M. M.; Sexton, P. M., Mechanisms of signalling and
710 biased agonism in G protein-coupled receptors. *Nat Rev Mol Cell Biol* **2018**, *19* (10), 638-653.
711 <https://doi.org/10.1038/s41580-018-0049-3>.
- 712 10. Flock, T.; Hauser, A. S.; Lund, N.; Gloriam, D. E.; Balaji, S.; Babu, M. M., Selectivity determinants of GPCR-G-
713 protein binding. *Nature* **2017**, *545* (7654), 317-322. <https://doi.org/10.1038/nature22070>.
- 714 11. Hofmann, K. P.; Scheerer, P.; Hildebrand, P. W.; Choe, H. W.; Park, J. H.; Heck, M.; Ernst, O. P., A G protein-
715 coupled receptor at work: the rhodopsin model. *Trends Biochem Sci* **2009**, *34* (11), 540-52.
716 <https://doi.org/10.1016/j.tibs.2009.07.005>.
- 717 12. Katritch, V.; Cherezov, V.; Stevens, R. C., Diversity and modularity of G protein-coupled receptor structures.
718 *Trends Pharmacol Sci* **2012**, *33* (1), 17-27. <https://doi.org/10.1016/j.tips.2011.09.003>.
- 719 13. Dror, R. O.; Green, H. F.; Valant, C.; Borhani, D. W.; Valcourt, J. R.; Pan, A. C.; Arlow, D. H.; Canals, M.; Lane,
720 J. R.; Rahmani, R.; Baell, J. B.; Sexton, P. M.; Christopoulos, A.; Shaw, D. E., Structural basis for modulation of a G-
721 protein-coupled receptor by allosteric drugs. *Nature* **2013**, *503* (7475), 295-9. <https://doi.org/10.1038/nature12595>.
- 722 14. Ye, L.; Van Eps, N.; Zimmer, M.; Ernst, O. P.; Prosser, R. S., Activation of the A2A adenosine G-protein-coupled
723 receptor by conformational selection. *Nature* **2016**, *533* (7602), 265-8. <https://doi.org/10.1038/nature17668>.
- 724 15. Schonegge, A. M.; Gallion, J.; Picard, L. P.; Wilkins, A. D.; Le Gouill, C.; Audet, M.; Stallaert, W.; Lohse, M. J.;
725 Kimmel, M.; Lichtarge, O.; Bouvier, M., Evolutionary action and structural basis of the allosteric switch controlling
726 beta2AR functional selectivity. *Nat Commun* **2017**, *8* (1), 2169. <https://doi.org/10.1038/s41467-017-02257-x>.
- 727 16. Latorraca, N. R.; Venkatakrishnan, A. J.; Dror, R. O., GPCR Dynamics: Structures in Motion. *Chem Rev* **2017**,
728 *117* (1), 139-155. <https://doi.org/10.1021/acs.chemrev.6b00177>.
- 729 17. Thal, D. M.; Glukhova, A.; Sexton, P. M.; Christopoulos, A., Structural insights into G-protein-coupled receptor
730 allostery. *Nature* **2018**, *559* (7712), 45-53. <https://doi.org/10.1038/s41586-018-0259-z>.
- 731 18. Venkatakrishnan, A. J.; Ma, A. K.; Fonseca, R.; Latorraca, N. R.; Kelly, B.; Betz, R. M.; Asawa, C.; Kobilka, B.
732 K.; Dror, R. O., Diverse GPCRs exhibit conserved water networks for stabilization and activation. *Proc Natl Acad Sci U S*
733 *A* **2019**, *116* (8), 3288-3293. <https://doi.org/10.1073/pnas.1809251116>.
- 734 19. Yuan, S.; Vogel, H.; Filipek, S., The role of water and sodium ions in the activation of the mu-opioid receptor.
735 *Angew Chem Int Ed Engl* **2013**, *52* (38), 10112-5. <https://doi.org/10.1002/anie.201302244>.
- 736 20. Nygaard, R.; Frimurer, T. M.; Holst, B.; Rosenkilde, M. M.; Schwartz, T. W., Ligand binding and micro-switches
737 in 7TM receptor structures. *Trends Pharmacol Sci* **2009**, *30* (5), 249-59. <https://doi.org/10.1016/j.tips.2009.02.006>.

- 738 21. Trzaskowski, B.; Latek, D.; Yuan, S.; Ghoshdastider, U.; Debinski, A.; Filipek, S., Action of molecular switches
739 in GPCRs--theoretical and experimental studies. *Curr Med Chem* **2012**, *19* (8), 1090-109.
- 740 22. Tehan, B. G.; Bortolato, A.; Blaney, F. E.; Weir, M. P.; Mason, J. S., Unifying family A GPCR theories of
741 activation. *Pharmacol Ther* **2014**, *143* (1), 51-60. <https://doi.org/10.1016/j.pharmthera.2014.02.004>.
- 742 23. Rasmussen, S. G.; DeVree, B. T.; Zou, Y.; Kruse, A. C.; Chung, K. Y.; Kobilka, T. S.; Thian, F. S.; Chae, P. S.;
743 Pardon, E.; Calinski, D.; Mathiesen, J. M.; Shah, S. T.; Lyons, J. A.; Caffrey, M.; Gellman, S. H.; Steyaert, J.; Skiniotis, G.;
744 Weis, W. I.; Sunahara, R. K.; Kobilka, B. K., Crystal structure of the beta2 adrenergic receptor-Gs protein complex. *Nature*
745 **2011**, *477* (7366), 549-55. <https://doi.org/10.1038/nature10361>.
- 746 24. Katritch, V.; Fenalti, G.; Abola, E. E.; Roth, B. L.; Cherezov, V.; Stevens, R. C., Allosteric sodium in class A
747 GPCR signaling. *Trends Biochem Sci* **2014**, *39* (5), 233-44. <https://doi.org/10.1016/j.tibs.2014.03.002>.
- 748 25. Bhattacharya, S.; Vaidehi, N., Differences in allosteric communication pipelines in the inactive and active states of
749 a GPCR. *Biophys J* **2014**, *107* (2), 422-434. <https://doi.org/10.1016/j.bpj.2014.06.015>.
- 750 26. Rodriguez, G. J.; Yao, R.; Lichtarge, O.; Wensel, T. G., Evolution-guided discovery and recoding of allosteric
751 pathway specificity determinants in psychoactive bioamine receptors. *Proc Natl Acad Sci U S A* **2010**, *107* (17), 7787-92.
752 <https://doi.org/10.1073/pnas.0914877107>.
- 753 27. Manglik, A.; Kim, T. H.; Masureel, M.; Altenbach, C.; Yang, Z.; Hilger, D.; Lerch, M. T.; Kobilka, T. S.; Thian, F.
754 S.; Hubbell, W. L.; Prosser, R. S.; Kobilka, B. K., Structural Insights into the Dynamic Process of beta2-Adrenergic
755 Receptor Signaling. *Cell* **2015**, *161* (5), 1101-1111. <https://doi.org/10.1016/j.cell.2015.04.043>.
- 756 28. Wescott, M. P.; Kufareva, I.; Paes, C.; Goodman, J. R.; Thaker, Y.; Puffer, B. A.; Berdugo, E.; Rucker, J. B.;
757 Handel, T. M.; Doranz, B. J., Signal transmission through the CXC chemokine receptor 4 (CXCR4) transmembrane helices.
758 *Proc. Natl. Acad. Sci. U. S. A.* **2016**, *113* (35), 9928-33. <https://doi.org/10.1073/pnas.1601278113>.
- 759 29. Furness, S. G. B.; Liang, Y. L.; Nowell, C. J.; Halls, M. L.; Wookey, P. J.; Dal Maso, E.; Inoue, A.; Christopoulos,
760 A.; Wootten, D.; Sexton, P. M., Ligand-Dependent Modulation of G Protein Conformation Alters Drug Efficacy. *Cell* **2016**,
761 *167* (3), 739-749 e11. <https://doi.org/10.1016/j.cell.2016.09.021>.
- 762 30. Sung, Y. M.; Wilkins, A. D.; Rodriguez, G. J.; Wensel, T. G.; Lichtarge, O., Intramolecular allosteric
763 communication in dopamine D2 receptor revealed by evolutionary amino acid covariation. *Proc Natl Acad Sci U S A* **2016**,
764 *113* (13), 3539-44. <https://doi.org/10.1073/pnas.1516579113>.
- 765 31. Vaidehi, N.; Bhattacharya, S., Allosteric communication pipelines in G-protein-coupled receptors. *Current*
766 *opinion in pharmacology* **2016**, *30*, 76-83. <https://doi.org/10.1016/j.coph.2016.07.010>.
- 767 32. Che, T.; Majumdar, S.; Zaidi, S. A.; Ondachi, P.; McCorvy, J. D.; Wang, S.; Mosier, P. D.; Uprety, R.; Vardy, E.;
768 Krumm, B. E.; Han, G. W.; Lee, M. Y.; Pardon, E.; Steyaert, J.; Huang, X. P.; Strachan, R. T.; Tribo, A. R.; Pasternak, G.
769 W.; Carroll, F. I.; Stevens, R. C.; Cherezov, V.; Katritch, V.; Wacker, D.; Roth, B. L., Structure of the Nanobody-Stabilized
770 Active State of the Kappa Opioid Receptor. *Cell* **2018**, *172* (1-2), 55-67 e15. <https://doi.org/10.1016/j.cell.2017.12.011>.
- 771 33. Eddy, M. T.; Lee, M. Y.; Gao, Z. G.; White, K. L.; Didenko, T.; Horst, R.; Audet, M.; Stanczak, P.; McClary, K.
772 M.; Han, G. W.; Jacobson, K. A.; Stevens, R. C.; Wuthrich, K., Allosteric Coupling of Drug Binding and Intracellular
773 Signaling in the A2A Adenosine Receptor. *Cell* **2018**, *172* (1-2), 68-80 e12. <https://doi.org/10.1016/j.cell.2017.12.004>.
- 774 34. Ngo, T.; Ilatovskiy, A. V.; Stewart, A. G.; Coleman, J. L.; McRobb, F. M.; Riek, R. P.; Graham, R. M.; Abagyan,
775 R.; Kufareva, I.; Smith, N. J., Orphan receptor ligand discovery by pickpocketing pharmacological neighbors. *Nat Chem*
776 *Biol* **2017**, *13* (2), 235-242. <https://doi.org/10.1038/nchembio.2266>.
- 777 35. Isberg, V.; Mordalski, S.; Munk, C.; Rataj, K.; Harpsøe, K.; Hauser, A. S.; Vroiling, B.; Bojarski, A. J.; Vriend, G.;
778 Gloriam, D. E., GPCRdb: an information system for G protein-coupled receptors. *Nucleic Acids Res* **2016**, *44* (D1), D356-
779 64. <https://doi.org/10.1093/nar/gkv1178>.
- 780 36. Valentin-Hansen, L.; Holst, B.; Frimurer, T. M.; Schwartz, T. W., PheVI:09 (Phe6.44) as a sliding microswitch in
781 seven-transmembrane (7TM) G protein-coupled receptor activation. *J Biol Chem* **2012**, *287* (52), 43516-26.
782 <https://doi.org/10.1074/jbc.M112.395137>.
- 783 37. Rovati, G. E.; Capra, V.; Neubig, R. R., The highly conserved DRY motif of class A G protein-coupled receptors:
784 beyond the ground state. *Mol Pharmacol* **2007**, *71* (4), 959-64. <https://doi.org/10.1124/mol.106.029470>.
- 785 38. Glukhova, A.; Draper-Joyce, C. J.; Sunahara, R. K.; Christopoulos, A.; Wootten, D.; Sexton, P. M., Rules of
786 engagement: GPCRs and G proteins. *ACS Pharmacology & Translational Science* **2018**.
787 <https://doi.org/10.1021/acspsci.8b00026>.

- 788 39. Hulme, E. C., GPCR activation: a mutagenic spotlight on crystal structures. *Trends Pharmacol Sci* **2013**, *34* (1),
789 67-84. <https://doi.org/10.1016/j.tips.2012.11.002>.
- 790 40. Erdelyi, L. S.; Mann, W. A.; Morris-Rosendahl, D. J.; Gross, U.; Nagel, M.; Varnai, P.; Balla, A.; Hunyady, L.,
791 Mutation in the V2 vasopressin receptor gene, AVPR2, causes nephrogenic syndrome of inappropriate diuresis. *Kidney Int*
792 **2015**, *88* (5), 1070-8. <https://doi.org/10.1038/ki.2015.181>.
- 793 41. Pasel, K.; Schulz, A.; Timmermann, K.; Linnemann, K.; Hoeltzenbein, M.; Jaaskelainen, J.; Gruters, A.; Filler, G.;
794 Schoneberg, T., Functional characterization of the molecular defects causing nephrogenic diabetes insipidus in eight
795 families. *J Clin Endocrinol Metab* **2000**, *85* (4), 1703-10. <https://doi.org/10.1210/jcem.85.4.6507>.
- 796 42. Napier, M. L.; Durga, D.; Wolsley, C. J.; Chamney, S.; Alexander, S.; Brennan, R.; Simpson, D. A.; Silvestri, G.;
797 Willoughby, C. E., Mutational Analysis of the Rhodopsin Gene in Sector Retinitis Pigmentosa. *Ophthalmic Genet* **2015**, *36*
798 (3), 239-43. <https://doi.org/10.3109/13816810.2014.958862>.
- 799 43. Wingler, L. M.; Elgeti, M.; Hilger, D.; Latorraca, N. R.; Lerch, M. T.; Staus, D. P.; Dror, R. O.; Kobilka, B. K.;
800 Hubbell, W. L.; Lefkowitz, R. J., Angiotensin Analogs with Divergent Bias Stabilize Distinct Receptor Conformations.
801 *Cell* **2019**, *176* (3), 468+. <https://doi.org/10.1016/j.cell.2018.12.005>.
- 802 44. Tan, L.; Yan, W.; McCorvy, J. D.; Cheng, J., Biased Ligands of G Protein-Coupled Receptors (GPCRs):
803 Structure-Functional Selectivity Relationships (SFSRs) and Therapeutic Potential. *J Med Chem* **2018**.
804 <https://doi.org/10.1021/acs.jmedchem.8b00435>.
- 805 45. Smith, J. S.; Lefkowitz, R. J.; Rajagopal, S., Biased signalling: from simple switches to allosteric microprocessors.
806 *Nat Rev Drug Discov* **2018**. <https://doi.org/10.1038/nrd.2017.229>.
- 807 46. Schmid, C. L.; Kennedy, N. M.; Ross, N. C.; Lovell, K. M.; Yue, Z. Z.; Morgenweck, J.; Cameron, M. D.;
808 Bannister, T. D.; Bohn, L. M., Bias Factor and Therapeutic Window Correlate to Predict Safer Opioid Analgesics. *Cell*
809 **2017**, *171* (5), 1165+. <https://doi.org/10.1016/j.cell.2017.10.035>.
- 810 47. Wootten, D.; Reynolds, C. A.; Smith, K. J.; Mobarec, J. C.; Koole, C.; Savage, E. E.; Pabreja, K.; Simms, J.;
811 Sridhar, R.; Furness, S. G.; Liu, M.; Thompson, P. E.; Miller, L. J.; Christopoulos, A.; Sexton, P. M., The Extracellular
812 Surface of the GLP-1 Receptor Is a Molecular Trigger for Biased Agonism. *Cell* **2016**, *165* (7), 1632-43.
813 <https://doi.org/10.1016/j.cell.2016.05.023>.
- 814 48. Lu, S.; Zhang, J., Small Molecule Allosteric Modulators of G-Protein-Coupled Receptors: Drug-Target
815 Interactions. *J Med Chem* **2018**. <https://doi.org/10.1021/acs.jmedchem.7b01844>.
- 816 49. Gregorio, G. G.; Masureel, M.; Hilger, D.; Terry, D. S.; Juette, M.; Zhao, H.; Zhou, Z.; Perez-Aguilar, J. M.;
817 Hauge, M.; Mathiasen, S.; Javitch, J. A.; Weinstein, H.; Kobilka, B. K.; Blanchard, S. C., Single-molecule analysis of
818 ligand efficacy in beta2AR-G-protein activation. *Nature* **2017**, *547* (7661), 68-73. <https://doi.org/10.1038/nature22354>.
- 819 50. Isogai, S.; Deupi, X.; Opitz, C.; Heydenreich, F. M.; Tsai, C. J.; Brueckner, F.; Schertler, G. F.; Veprintsev, D. B.;
820 Grzesiek, S., Backbone NMR reveals allosteric signal transduction networks in the beta1-adrenergic receptor. *Nature* **2016**,
821 *530* (7589), 237-41. <https://doi.org/10.1038/nature16577>.
- 822 51. Lee, M. H.; Appleton, K. M.; Strungs, E. G.; Kwon, J. Y.; Morinelli, T. A.; Peterson, Y. K.; Laporte, S. A.;
823 Luttrell, L. M., The conformational signature of beta-arrestin2 predicts its trafficking and signalling functions. *Nature* **2016**,
824 *531* (7596), 665-8. <https://doi.org/10.1038/nature17154>.
- 825 52. Tian, H.; Furstenberg, A.; Huber, T., Labeling and Single-Molecule Methods To Monitor G Protein-Coupled
826 Receptor Dynamics. *Chem Rev* **2017**, *117* (1), 186-245. <https://doi.org/10.1021/acs.chemrev.6b00084>.
- 827 53. Dror, R. O.; Pan, A. C.; Arlow, D. H.; Borhani, D. W.; Maragakis, P.; Shan, Y.; Xu, H.; Shaw, D. E., Pathway and
828 mechanism of drug binding to G-protein-coupled receptors. *Proc Natl Acad Sci U S A* **2011**, *108* (32), 13118-23.
829 <https://doi.org/10.1073/pnas.1104614108>.
- 830 54. Hauser, A. S.; Chavali, S.; Masuho, I.; Jahn, L. J.; Martemyanov, K. A.; Gloriam, D. E.; Babu, M. M.,
831 Pharmacogenomics of GPCR Drug Targets. *Cell* **2018**, *172* (1-2), 41-54 e19. <https://doi.org/10.1016/j.cell.2017.11.033>.
- 832 55. Pandy-Szekeres, G.; Munk, C.; Tsonkov, T. M.; Mordalski, S.; Harpsoe, K.; Hauser, A. S.; Bojarski, A. J.;
833 Gloriam, D. E., GPCRdb in 2018: adding GPCR structure models and ligands. *Nucleic Acids Res* **2018**, *46* (D1), D440-
834 D446. <https://doi.org/10.1093/nar/gkx1109>.
- 835 56. Capra, J. A.; Singh, M., Predicting functionally important residues from sequence conservation. *Bioinformatics*
836 **2007**, *23* (15), 1875-82. <https://doi.org/10.1093/bioinformatics/btm270>.

- 837 57. Mirny, L. A.; Shakhnovich, E. I., Universally conserved positions in protein folds: reading evolutionary signals
838 about stability, folding kinetics and function. *J Mol Biol* **1999**, *291* (1), 177-96. <https://doi.org/10.1006/jmbi.1999.2911>.
- 839 58. The UniProt, C., UniProt: the universal protein knowledgebase. *Nucleic Acids Res* **2017**, *45* (D1), D158-D169.
840 <https://doi.org/10.1093/nar/gkw1099>.
- 841 59. Amberger, J.; Bocchini, C.; Hamosh, A., A new face and new challenges for Online Mendelian Inheritance in Man
842 (OMIM(R)). *Human mutation* **2011**, *32* (5), 564-7. <https://doi.org/10.1002/humu.21466>.
- 843 60. Zerbino, D. R.; Achuthan, P.; Akanni, W.; Amode, M. R.; Barrell, D.; Bhai, J.; Billis, K.; Cummins, C.; Gall, A.;
844 Giron, C. G.; Gil, L.; Gordon, L.; Haggerty, L.; Haskell, E.; Hourlier, T.; Izuogu, O. G.; Janacek, S. H.; Juettemann, T.; To,
845 J. K.; Laird, M. R.; Lavidas, I.; Liu, Z.; Loveland, J. E.; Maurel, T.; McLaren, W.; Moore, B.; Mudge, J.; Murphy, D. N.;
846 Newman, V.; Nuhn, M.; Ogeh, D.; Ong, C. K.; Parker, A.; Patricio, M.; Riat, H. S.; Schuilenburg, H.; Sheppard, D.;
847 Sparrow, H.; Taylor, K.; Thormann, A.; Vullo, A.; Walts, B.; Zadissa, A.; Frankish, A.; Hunt, S. E.; Kostadima, M.;
848 Langridge, N.; Martin, F. J.; Muffato, M.; Perry, E.; Ruffier, M.; Staines, D. M.; Trevanion, S. J.; Aken, B. L.; Cunningham,
849 F.; Yates, A.; Flicek, P., Ensembl 2018. *Nucleic Acids Res* **2018**, *46* (D1), D754-D761. <https://doi.org/10.1093/nar/gkx1098>.
- 850 61. Beard, H.; Cholleti, A.; Pearlman, D.; Sherman, W.; Loving, K. A., Applying physics-based scoring to calculate
851 free energies of binding for single amino acid mutations in protein-protein complexes. *PLoS One* **2013**, *8* (12), e82849.
852 <https://doi.org/10.1371/journal.pone.0082849>.
- 853 62. Isberg, V.; de Graaf, C.; Bortolato, A.; Cherezov, V.; Katritch, V.; Marshall, F. H.; Mordalski, S.; Pin, J. P.;
854 Stevens, R. C.; Vriend, G.; Gloriam, D. E., Generic GPCR residue numbers - aligning topology maps while minding the
855 gaps. *Trends Pharmacol Sci* **2015**, *36* (1), 22-31. <https://doi.org/10.1016/j.tips.2014.11.001>.
- 856 63. Ballesteros, J. A.; Weinstein, H., Integrated methods for the construction of three-dimensional models and
857 computational probing of structure-function relations in G protein coupled receptors. In *Receptor Molecular Biology*,
858 Sealfon, S. C., Ed. Academic Press: 1995; Vol. 25, pp 366-428.
- 859 64. Eldridge, M. D.; Murray, C. W.; Auton, T. R.; Paolini, G. V.; Mee, R. P., Empirical scoring functions: I. The
860 development of a fast empirical scoring function to estimate the binding affinity of ligands in receptor complexes. *Journal*
861 *of computer-aided molecular design* **1997**, *11* (5), 425-45.
- 862 65. Verdonk, M. L.; Cole, J. C.; Hartshorn, M. J.; Murray, C. W.; Taylor, R. D., Improved protein-ligand docking
863 using GOLD. *Proteins* **2003**, *52* (4), 609-23. <https://doi.org/10.1002/prot.10465>.
- 864 66. Wang, S.; Sun, S.; Li, Z.; Zhang, R.; Xu, J., Accurate De Novo Prediction of Protein Contact Map by Ultra-Deep
865 Learning Model. *PLoS Comput Biol* **2017**, *13* (1), e1005324. <https://doi.org/10.1371/journal.pcbi.1005324>.
- 866 67. Kufareva, I.; Abagyan, R., Methods of Protein Structure Comparison. In *Homology Modeling: Methods and*
867 *Protocols*, Orry, A. J. W.; Abagyan, R., Eds. Humana Press: Totowa, NJ, 2012; pp 231-257.
- 868 68. Kufareva, I.; Rueda, M.; Katritch, V.; Stevens, R. C.; Abagyan, R.; participants, G. D., Status of GPCR modeling
869 and docking as reflected by community-wide GPCR Dock 2010 assessment. *Structure* **2011**, *19* (8), 1108-26.
870 <https://doi.org/10.1016/j.str.2011.05.012>.
- 871 69. Marsden, B.; Abagyan, R., SAD--a normalized structural alignment database: improving sequence-structure
872 alignments. *Bioinformatics* **2004**, *20* (15), 2333-44. <https://doi.org/10.1093/bioinformatics/bth244>.
- 873 70. Jones, T. A.; Zou, J. Y.; Cowan, S. W.; Kjeldgaard, M., Improved methods for building protein models in electron
874 density maps and the location of errors in these models. *Acta Crystallogr A* **1991**, *47* (Pt 2), 110-9.
875 <https://doi.org/10.1107/s0108767390010224>.
- 876 71. Smart, O. S.; Horsky, V.; Gore, S.; Svobodova Varekova, R.; Bendova, V.; Kleywegt, G. J.; Velankar, S.,
877 Validation of ligands in macromolecular structures determined by X-ray crystallography. *Acta Crystallogr D Struct Biol*
878 **2018**, *74* (Pt 3), 228-236. <https://doi.org/10.1107/S2059798318002541>.
- 879 72. Kleywegt, G. J.; Harris, M. R.; Zou, J. Y.; Taylor, T. C.; Wahlby, A.; Jones, T. A., The Uppsala Electron-Density
880 Server. *Acta Crystallogr D Biol Crystallogr* **2004**, *60* (Pt 12 Pt 1), 2240-9. <https://doi.org/10.1107/S0907444904013253>.
- 881 73. Crooks, G. E.; Hon, G.; Chandonia, J. M.; Brenner, S. E., WebLogo: a sequence logo generator. *Genome research*
882 **2004**, *14* (6), 1188-90. <https://doi.org/10.1101/gr.849004>.
- 883 74. Vassart, G.; Costagliola, S., G protein-coupled receptors: mutations and endocrine diseases. *Nat Rev Endocrinol*
884 **2011**, *7* (6), 362-72. <https://doi.org/10.1038/nrendo.2011.20>.

- 885 75. Thompson, M. D.; Hendy, G. N.; Percy, M. E.; Bichet, D. G.; Cole, D. E., G protein-coupled receptor mutations
886 and human genetic disease. *Methods Mol Biol* **2014**, *1175*, 153-87. https://doi.org/10.1007/978-1-4939-0956-8_8.
- 887 76. Tao, Y. X., Inactivating mutations of G protein-coupled receptors and diseases: structure-function insights and
888 therapeutic implications. *Pharmacol Ther* **2006**, *111* (3), 949-73. <https://doi.org/10.1016/j.pharmthera.2006.02.008>.
- 889 77. Tao, Y. X., Constitutive activation of G protein-coupled receptors and diseases: insights into mechanisms of
890 activation and therapeutics. *Pharmacol Ther* **2008**, *120* (2), 129-48. <https://doi.org/10.1016/j.pharmthera.2008.07.005>.
- 891 78. Massink, A.; Gutierrez-de-Teran, H.; Lenselink, E. B.; Ortiz Zacarias, N. V.; Xia, L.; Heitman, L. H.; Katritch, V.;
892 Stevens, R. C.; AP, I. J., Sodium ion binding pocket mutations and adenosine A2A receptor function. *Mol Pharmacol* **2015**,
893 *87* (2), 305-13. <https://doi.org/10.1124/mol.114.095737>.